David Holder's Bumper Book of EIT

February 2, 2004

Chapter 1

The Reconstruction Problem

William Lionheart, Nicholas Polydorides and Andrea Borsic

1.1 Why is EIT so hard?

In conventional medical imaging modalities, such as X-Ray computerized tomography, a collimated beam of radiation passes through the object in a straight line, and the attenuation of this beam is affected only by the matter which lies along its path. In this sense X-Ray CT is *local*, and it means that the pixels or voxels of our image affect only some (in fact a very small proportion) of the measurements. If the radiation were at lower frequency (*softer* X-rays) the effect of scattering would have to be taken into account and the effect of a change of material in a voxel would no longer be local. As the frequency decreases this nonlocal effect becomes more pronounced until we reach the case of direct current, in which a change in conductivity would have some effect on any measurement of surface voltage when any current pattern is applied. This *non-local* property of conductivity imaging, which still applies at the moderate frequencies used in EIT, is one of the principle reasons that EIT is difficult. It means that to find the conductivity image one must solve a system of simultaneous equations relating every voxel to every measurement.

Non-locality in itself is not such a big problem provided we attempt to recover a modest number of unknown conductivity parameters from a modest number of measurements. Worse than that is the ill-posed nature of the problem. According to Hadamard a mathematical model of a physical problem is well posed if

1) For all admissible data, a solution exists.

2) For all admissible data, the solution is unique.

3) The solution depends continuously on the data.

The problem of recovering an unknown conductivity from boundary data is severely ill-posed, and it is the third criterion which gives us the most trouble. In practice that means for any given measurement precision, there are arbitrarily large changes in the conductivity distribution which are undetectable by boundary voltage measurements at that precision. This is clearly bad news for practical low frequency electrical imaging. Before we give up EIT altogether and take up market gardening, there is a partial answer to this problem — we need some additional information about the conductivity distribution. If we know enough *a priori* (that is in advance) information, it constrains the solution so that the wild variations causing the instability are ruled out.

The other two criteria can be phrased in a more practical way for our problem. Existence of a solution is not really in question. We believe the body has a conductivity. The issue is more that the data is sufficiently accurate to be consistent with a conductivity distribution. Small errors in measurement can violate consistency conditions, such as reciprocity. One way around this is to project our infeasible data on to the closest feasible set. The mathematician's problem of uniqueness of solution is better understood in experimental terms as sufficiency of data. In the mathematical literature the conductivity inverse boundary value problem (or Calderón problem) is to show that a complete knowledge of the relationship between voltage and current at the boundary determines the conductivity uniquely. This has been proved under a variety of assumptions about the smoothness of the conductivity [75]. This is only a partial answer to the practical problem as we have only finitely many measurements from a fixed system of electrodes, the electrodes typically cover only a portion of the surface of the body and in many cases voltage are not measured on electrodes driving currents. In the practical case the number of degrees of freedom of a parameterized conductivity we can recover is limited by the number of independent measurements made and the accuracy of those measurements.

This introductory section has deliberately avoided mathematical treatment, but a further understanding of why the reconstruction problem of EIT is difficult, and how it might be done requires some mathematical prerequisites. The minimum required for the following is reasonably thorough understanding of matrices [136], and little multi-variable calculus, such as are generally taught to engineering undergraduates. For those desirous of a deeper knowledge of EIT reconstruction, for example those wishing to implement reconstruction software, an undergraduate course in the finite element method [129] and another in inverses problems [19, 20, 67] would be advantageous.

1.2 Mathematical Setting

Our starting point for consideration of EIT should be Maxwell's equations. But for simplicity let us assume direct current or sufficiently low a frequency current that the magnetic field can be neglected. We have a given body Ω a

closed and bounded subset of three-dimensional space with a smooth (or smooth enough) boundary $\partial\Omega$. The body has a conductivity σ which is a function of the spatial variable $\mathbf{x}$ (although we will not always make this dependence explicit for simplicity of notation). The scalar potential is ϕ and the electric field is $\mathbf{E} = -\nabla\phi$. The current density is $\mathbf{J} = -\sigma\nabla\phi$, which is a continuum version of Ohm's law. In the absence of interior current sources, we have the continuum Kirchoff's law[1]

$$\nabla \cdot \sigma\nabla\phi = 0 \tag{1.1}$$

The current density on the boundary is

$$j = -\mathbf{J} \cdot \mathbf{n} = \sigma\nabla\phi \cdot \mathbf{n}$$

where $\mathbf{n}$ is the outward unit normal to $\partial\Omega$. Given σ, specification of the potential $\phi|_{\partial\Omega}$ on the boundary (Dirichlet boundary condition) is sufficient to uniquely determine a solution ϕ to (1.1). Similarly specification of boundary current density j (Neumann boundary conditions) determines ϕ up to an additive constant, which is equivalent to choosing an earth point. From Gauss' theorem, or conservation of current, the boundary current density must satisfy the consistency condition $\int_{\partial\Omega} j = 0$. The ideal complete data in the EIT reconstruction problem is to know all possible pairs of Dirichlet and Neumann data $\phi|_{\partial\Omega}, j$. As any Dirichlet data determines unique Neumann data we have an operator $\Lambda_\sigma : \phi|_{\partial\Omega} \mapsto j$. In electrical terms this operator is the transconductance at the boundary, and can be regarded as the response of the system we are electrically interrogating at the boundary.

Practical EIT systems use sinusoidal currents at fixed angular frequency ω The electric field, current density and potential are all represented by complex phasers multiplied by $e^{i\omega}$. Ignoring magnetic effects (See Box 1.2) we replace the conductivity σ in 1.1 by the complex *admittivity* $\gamma = \sigma + i\omega\varepsilon$ where ε is the permittivity. In biological tissue one can expect ε to be frequency dependent which becomes important in a multi-frequency system (X-REF).

[1] There is a recurring error in the EIT literature of calling this Poisson's equation, it however a natural generalisation of Laplace's equation

Box 1.1: Maxwell's Equations

In the main text we have treated essentially the direct current case.The basic field quantities in Maxwell's equations are the electric field $\mathbf{E}$ and the magnetic field $\mathbf{H}$ which will be modelled as vector valued functions of space and time. We will assume that there is no relative motion in our system. The fields, when applied to a material or indeed a vacuum, produce fluxes – electric displacement $\mathbf{D}$ and magnetic flux $\mathbf{B}$. The spacial and temporal variations of the fields and fluxes are linked by Faraday's Law of induction

$$\nabla \times \mathbf{E} = -\frac{\partial \mathbf{B}}{\partial t}$$

and Coulomb's law

$$\nabla \times \mathbf{H} = \frac{\partial \mathbf{D}}{\partial t} + \mathbf{J}$$

where $\mathbf{J}$ is the electric current density. We define the charge density by $\nabla \cdot \mathbf{E} = \rho$, and as there are no magnetic monopoles $\nabla \cdot \mathbf{B} = 0$. The material properties appear as relations between fields and fluxes. The simplest case is of non-dispersive, local, linear, isotropic media. The magnetic permeability is then a scalar function $\mu > 0$ of space and the material response is $\mathbf{B} = \mu\mathbf{H}$, and similarly the permittivity $\varepsilon > 0$ with $\mathbf{D} = \varepsilon\mathbf{E}$. In a conductive medium we have the continuum counterpart to Ohm's law where the conduction current density $\mathbf{J_c} = \sigma\mathbf{E}$. The total current is then $\mathbf{J} = \mathbf{J_c} + \mathbf{J_s}$ the sum of the conduction and source currents.
We will write $\mathbf{E}(\mathbf{x}, t) = \mathrm{Re}(\mathbf{E}(\mathbf{x})\mathrm{e}^{\mathrm{i}\omega t})$ where $\mathbf{E}(\mathbf{x})$ is a complex vector valued function of space. We now have the time harmonic Maxwell's equations

$$\nabla \times \mathbf{E} = -\mathrm{i}\omega\mu\mathbf{H}$$

$$\nabla \times \mathbf{H} = \mathrm{i}\omega\varepsilon\mathbf{E} + \mathbf{J} \qquad (\dagger)$$

We can combine conductivity and permittivity as a complex admittivity $\sigma + \mathrm{i}\omega\varepsilon$ and write $(\dagger)$ as

$$\nabla \times \mathbf{H} = (\sigma + \mathrm{i}\omega\varepsilon)\mathbf{E} + \mathbf{J_s}$$

In EIT typically the source term $\mathbf{J_s}$ is zero at frequency ω. The quasi-static approximation usually employed in EIT is to assume $\omega\mu\mathbf{H}$ is negligible so that $\nabla \times \mathbf{E} = 0$ and hence on a simply connected domain $\mathbf{E} = -\nabla\phi$ for a scalar ϕ.

Box 1.2: Sobolev Spaces

In the mathematical literature you will often see the assumption that ϕ lies in the Sobolev Space $H^1(\Omega)$, which can look intimidating to the uninitiated. Actually these spaces are easily understood on an intuitive level and have a natural physical meaning. For mathematical details see Folland [48]. A (generalized) function f is in $H^k(\Omega)$ for integer k if the square kth derivative has a finite integral over Ω. For non-integer and negative powers Sobolev spaces are defined by taking the Fourier transform, multiplying by a power of frequency and demanding that the result is square integrable. For the potential we are simply demanding that $\int_\Omega |\nabla\phi|^2\, dV < \infty$ which is equivalent, provided the conductivity is bounded, to demanding that the ohmic power dissipated is finite. An obviously necessary physical constraint. Sobolev spaces are useful as a measure of the smoothness of a function, and are also convenient as they have an inner product (they are Hilbert spaces). To be consistent with this finite power condition the Dirichlet boundary data $\phi|_{\partial\Omega}$ must be in $H^{1/2}(\partial\Omega)$ and the Neumann data $j \in H^{-1/2}(\partial\Omega)$. Note that the current density is one derivative less smooth than the potential on the boundary as one might expect.

The inverse problem, as formulated by Calderón [28], is to recover σ from Λ_σ. The uniqueness of solution, or if you like the sufficiency of the data, has been shown under a variety of assumptions, notably in the work of Kohn and Vogelius [78] and Sylvester and Uhlmann [138]. For a summary of results see Isakov [75]. More recently Astala and Paivarinta [1] have shown uniqueness for the 2D case without smoothness assumptions. There is very little theoretical work on what can be determined from incomplete data, but knowing the Dirichlet to Neumann mapping on an open subset of the boundary is enough [142]. It is also known that one set of Dirichlet and Neumann data, provided it contains enough frequency components, is enough to determine the boundary between two homogeneous materials with differing conductivities [2]. These results show that the second of Hadamard's conditions is not the problem, at least in the limiting, 'infinitely many electrodes' case. As for the first of Hadamard's condition, the difficulty is characterising 'admissible data' and there is very little work characterising what operators are valid Dirichlet-to-Neumann operators. The real problem however is in the third of Hadamard's conditions. In the absence of *a priori* information about the conductivity, the inverse problem $\Lambda_\sigma \mapsto \sigma$ is extremely unstable in the presence of noise. To understand this problem further it is best to use a simple example. Let us consider a unit disk in two dimensions with a concentric circular anomaly in the conductivity

$$\sigma(\mathbf{x}) = \begin{cases} \sigma_1 & \rho < |\mathbf{x}| < 1 \\ \sigma_2 & |\mathbf{x}| \le \rho \end{cases} .$$

Although this is a two dimensional example, it is equivalent to a three dimensional cylinder with a central cylindrical anomaly provided we consider only

data where the current density is zero on the circular faces of the cylinder and translationally invariant on the curved face (think of electrodes running the full height of a cylindrical tank).

The forward problem can be solved by separation of variables giving

$$\Lambda_\sigma[\cos k\theta] = k\frac{1+\mu\rho^{2k}}{1-\mu\rho^{2k}}\cos k\theta \tag{1.2}$$

and similarly for sin, where $\mu = (\sigma_1 - \sigma_2)/(\sigma_1 + \sigma_2)$. We can now express any arbitrary Dirichlet boundary data as a Fourier series $\phi(1,\theta) = \sum_k^\infty a_k \cos k\theta + b_k \sin k\theta$ and notice that the Fourier coefficients of the current density be $k(1+\mu\rho^{2k})/(1-\mu\rho^{2k})a_k$ and similarly b_k. The lowest frequency component is clearly most sensitive to the variation in the conductivity of the anomaly. This of itself is a useful observation indicating that patterns of voltage (or current) with large low frequency components are best able to detect an object near the centre of the domain. This might be achieved for example by covering a large proportion of the surface with driven electrodes and exciting a voltage or current pattern with low spacial frequency. We will explore this further in Section 1.9.3. We can understand a crucial feature of the non-linearity of EIT from this simple example - saturation. Fixing the radius of the anomaly and varying the conductivity we see that for high contrasts from the effect on the voltage of further varying the conductivity is reduced. A detailed analysis of the circular anomaly was performed by Seagar[126] using conformal mappings, including offset anomalies. It is found of course that central anomaly produces the least change in boundary data. This illustrates the positional dependence on the sensitivity of EIT to detect an object. By analogy to conventional imaging problems one could say that the 'point spread function' is position dependent.

Our central circular anomaly also demonstrates the ill-posed nature of the problem. For a given level of measurement precision, we can construct a circular anomaly undetectable at that precision. We can make the change in conductivity arbitrarily large and yet by reducing the radius we are still not be able to detect the anomaly. This shows (at least using the rather severe L^∞ norm that Hadamard's 3rd condition is violated.

1.3 Measurements and electrodes

A typical electrical imaging system uses a system of conducting electrodes attached to the surface of the body under investigation. One can apply current or voltage to these electrodes and measure voltage or current respectively. Let us suppose that the subset of the boundary in contact with the l-th electrode is E_l, and $1 \le l \le L$. For one particular measurement the voltages (with respect to some arbitrary reference) are V_l and the currents I_l, which we arrange in vectors [2] as $\mathbf{V}$ and $\mathbf{I} \in \mathbb{C}^L$. The discrete equivalent of the Dirichlet-to-Neumann Λ map

[2]Here $\mathbb{C}^n$ is the set of complex column vectors with n rows, whereas $\mathbb{C}^{m\times n}$ is the set of complex $m \times n$ matrices

is the transfer admittance, or mutual admittance, matrix $\mathbf{Y}$ which is defined by $\mathbf{I} = \mathbf{YV}$.

Assuming that the electrodes are perfect conductors for each l we have that $\phi|_{E_l} = V_l$, a constant. Away from the electrodes where no current flows $\partial\phi/\partial\mathbf{n} = 0$. This mixed boundary value problem is well-posed, and the resulting currents are $I_l = \int_{E_l} \sigma\partial\phi/\partial\mathbf{n}$. It is easy to see that the vector $\mathbf{1} = (1, 1, \ldots, 1)^T$ is in the null space of $\mathbf{Y}$, and that the range of $\mathbf{Y}$ is orthogonal to the same vector. Let S be the subspace of $\mathbb{C}^L$ perpendicular to $\mathbf{1}$ then it can be shown that $\mathbf{Y}|_S$ is invertible from S to S. The generalized inverse (see Sec 1.4) $\mathbf{Z} = \mathbf{Y}^\dagger$ is called the transfer impedance. This follows from uniqueness of solution of the so called *shunt model* boundary value problem, which is (1.1) together with the boundary conditions

$$\int_{E_l} \sigma\partial\phi/\partial\mathbf{n} = I_l \text{ for } 0 \leq l \leq L \tag{1.3}$$

$$\partial\phi/\partial\mathbf{n} = 0, \text{ on } \Gamma' \tag{1.4}$$

$$\nabla\phi \times \mathbf{n} = 0 \text{ on } \Gamma \tag{1.5}$$

where $\Gamma = \bigcup_l E_l$ and $\Gamma' = \partial\Omega - \Gamma$. The last condition (1.5) is equivalent to demanding that ϕ is constant on electrodes.

The transfer admittance, or equivalently impedance represents a complete set of data which can be collected from the L electrodes at a single frequency for a stationary linear medium. From reciprocity we have that $\mathbf{Y}$ and $\mathbf{Z}$ are symmetric (but for $\omega \neq 0$ *not Hermittian*). The dimension of the space of possible transfer admittance matrices is clearly no bigger than $L(L-1)/2$, and so it is unrealistic to expect to recover more unknown parameters than this. In the case of planar resistor networks the possible transfer admittance matrices can be characterized completely [39], a characterization which is known at least partly to hold in the planar continuum case [72]. A typical electrical imaging system applies current or voltage patterns which form a basis of the space S, and measures some subset of the resulting voltages which as they are only defined up to an additive constant can be taken to be in S.

The shunt model with its idealization of perfectly conducting electrodes predicts that the current density on the electrode has a singularity of the form $O(r^{-1/2})$ where r is the distance from the edge of the electrode. The potential ϕ while still continuous near the electrode has the asymptotics $O(r^{1/2})$. Although some electrodes may have total current $I_l = 0$ as they are not actively driven the shunting effect means that their current density is not only non-zero but infinite at the edges.

In medical application with electrodes applied to skin, and in phantom tanks with ionic solutions in contact with metal electrodes a contact impedance layer exists between the solution or skin and the electrode. This modifies the shunting effect so that the voltage under the electrode is no longer constant. The voltage on the electrode is still a constant V_l so now on E_l there is a voltage drop across

the contact impedance layer

$$\phi + z_l \sigma \frac{\partial \phi}{\partial \mathbf{n}} = V_l \tag{1.6}$$

where the contact impedance z_l could vary over E_l but is generally assumed constant. This new boundary condition together with (1.3) and (1.4) form the *Complete Electrode Model* or CEM. For experimental validation of this model see [34], theory [134] and numerical calculations [110, 146]. A nonzero contact impedance removes the singularity in the current density, although high current densities still occur at the edges of electrodes (fig 1.1). For asymptotics of ϕ with the CEM see [42].

The singular values (see 1.4.3) of $\mathbf{Z}$ sometimes called *characteristic impedances* are sensitive to the electrode model used and this was used by [34] to validate the CEM. With no modelling of electrodes and a rotationally symmetric conductivity in a cylindrical tank, the characteristic impedances tend toward a $1/k$ decay, as expected from (1.2) with sinusoidal singular vectors of frequency k, as the number of electrodes increases.

1.4 Regularizing Linear Illposed problems

In this section we consider the general problem of solving a linear illposed problem, before applying this specifically to EIT in the next section. Detailed theory and examples of linear ill-posed problems can be found in [140, 20, 151, 67, 45]. We assume a background in basic linear algebra [136]. For complex vectors $\mathbf{x} \in \mathbb{C}^n$ and $\mathbf{b} \in \mathbb{C}^m$ and a complex matrix $\mathbf{A} \in \mathbb{C}^{m \times n}$ we wish to find $\mathbf{x}$ given $\mathbf{A}\mathbf{x} = \mathbf{b}$. Of course in our case $\mathbf{A}$ is the Jacobian while $\mathbf{x}$ will be a conductivity change and $\mathbf{b}$ a voltage error. In practical measurement problems it is usual to have more data than unknowns, and if the surfeit of data were are only problem the natural solution would be to use the Moore-Penrose generalized inverse

$$\mathbf{x}_{\mathrm{MP}} = \mathbf{A}^{\dagger}\mathbf{b} = (\mathbf{A}^*\mathbf{A})^{-1}\mathbf{A}^*\mathbf{b} \tag{1.7}$$

which is the *least squares solution* in that

$$\mathbf{x}_{\mathrm{MP}} = \arg\min_{\mathbf{x}} ||\mathbf{A}\mathbf{x} - \mathbf{b}|| \tag{1.8}$$

(here $\arg\min_{\mathbf{x}}$ means the argument $\mathbf{x}$ which minimizes what follows). In MATLAB[3] the backslash (left division) operator can be used to calculate the lease squares solution, for example $x = A\backslash b$.

[3]MATLAB®is a matrix oriented interpreted programming language for numerical calculation (The MathWorks Inc, Natick, MA, USA). While we write MATLAB for brevity we include its free relatives Scilab and Octave

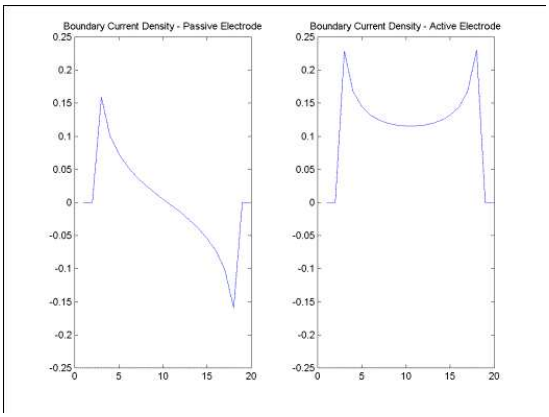

(a) Current density on the boundary for passive and active electrodes

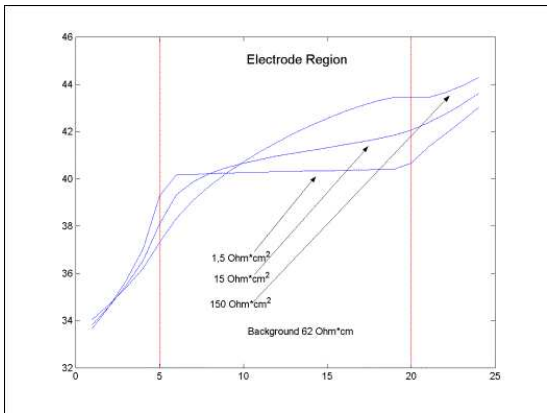

(b) The effect of contact impedance on the potential beneath an electrode

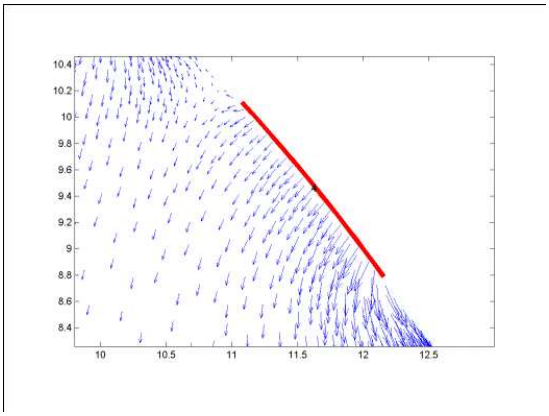

(c) Interior current flux near an active electrode

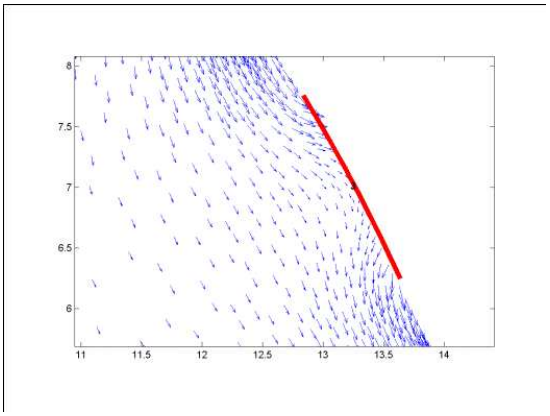

(d) Interior current flux near a passive electrode

Figure 1.1: The current density on the boundary with the CEM is greatest at the edge of the electrodes, even for passive electrodes. This effect is reduced as the contact impedance increases.

1.4.1 Ill-conditioning

It is the third of Hadamard's conditions, instability which causes us problems. To understand this first we define the operator norm of a matrix

$$\|A\| = \max_{\mathbf{x}\neq\mathbf{0}} \frac{\|\mathbf{A}\mathbf{x}\|}{\|\mathbf{x}\|}.$$

This can be calculated as the square root of the largest eigenvalue of $\mathbf{A}^*\mathbf{A}$. There is another norm on matrices in $\mathbb{C}^{m\times n}$ the *Frobenious norm* which is simply

$$\|\mathbf{A}\|_F^2 = \sum_{i=1}^{m}\sum_{j=1}^{n} |a_{ij}|^2 = \text{trace}\mathbf{A}^*\mathbf{A}$$

which treats the matrix as simply a vector rater than an operator. We also define the condition number

$$\kappa(\mathbf{A}) = \|\mathbf{A}\| \cdot \|\mathbf{A}^{-1}\|.$$

for $\mathbf{A}$ invertible. Assuming that $\mathbf{A}$ is known accurately, $\kappa(\mathbf{A})$ measures the amplification of relative error in the solution.

Specifically if

$$\mathbf{A}\mathbf{x} = \mathbf{b} \quad \text{and} \quad \mathbf{A}(\mathbf{x}+\delta\mathbf{x}) = \mathbf{b} + \delta\mathbf{b}$$

then the relative error in solution and data are related by

$$\frac{\|\delta\mathbf{x}\|}{\|\mathbf{x}\|} \leq \kappa(\mathbf{A}) \frac{\|\delta\mathbf{b}\|}{\|\mathbf{b}\|}$$

as can be easily shown from the definition of operator norm. Note that this is a 'worst case' error bound, often the error is less. With infinite precision, any finite $\kappa(\mathbf{A})$ shows that $\mathbf{A}^{-1}$ is continuous, but in practice error in data could be amplified so much the solution is useless. Even if the data $\mathbf{b}$ were reasonably accurate, numerical errors mean that, effectively $\mathbf{A}$ has error, and

$$\frac{\|\delta\mathbf{x}\|}{\|\mathbf{x}\|} \leq \kappa(\mathbf{A}) \frac{\|\delta\mathbf{A}\|}{\|\mathbf{A}\|}.$$

(Actually this is not quite honest, it should be a 'perturbation bound' see [70].) So in practice we can regard linear problems with large $\kappa(A)$ as 'ill-posed' although the term *ill-conditioned* is better for the discrete case.

1.4.2 Tikhonov Regularization

The method commonly known as Tikhonov Regularization was introduced to solve integral equations by Phillips [113] and Tikhonov [141] and for finite dimensional problems by Hoerl [71]. In the statistical literature, following Hoerl, the technique is know as *ridge regression*. We will explain it here for the finite

dimensional case. The least squares approach fails for a badly conditioned $\mathbf{A}$ but one strategy is to replace the least squares solution by

$$\mathbf{x}_\alpha = \arg\min_{\mathbf{x}} \quad \|\mathbf{A}\mathbf{x} - \mathbf{b}\|^2 + \alpha^2\|\mathbf{x}\|^2. \tag{1.9}$$

Here we trade off actually getting a solution to $\mathbf{A}\mathbf{x} = \mathbf{b}$ and not letting $\|\mathbf{x}\|$ get too big. The number α controls this trade-off and is called a *regularization parameter*. Notice that as $\alpha \to 0$, $\mathbf{x}_\alpha$ tends to a generalized solution $\mathbf{A}^\dagger\mathbf{b}$. It is easy to find an explicit formula for the minimum

$$\mathbf{x}_\alpha = (\mathbf{A}^*\mathbf{A} + \alpha^2\mathbf{I})^{-1}\mathbf{A}^*\mathbf{b}.$$

The condition number $\kappa((\mathbf{A}^*\mathbf{A} + \alpha^2\mathbf{I})^{-1})$ is $\frac{\lambda_1+\alpha^2}{\lambda_n+\alpha^2}$ where λ_i are the eigenvalues of $\mathbf{A}^*\mathbf{A}$, which for λ_n small is close to $\frac{\lambda_1}{\alpha^2} + 1$, so for big α it is well conditioned. Notice also see that even if $\mathbf{A}$ does not have full rank ($\lambda_n = 0$), $\mathbf{A}^*\mathbf{A} + \alpha^2\mathbf{I}$ does.

1.4.3 The Singular Value Decomposition

The singular value decomposition (SVD) is the generalization to non-square matrices of orthogonal diagonalization of Hermittian matrices. We describe the SVD in some detail here due to its importance in EIT. Although the topic is often neglected in elementary linear algebra courses and texts ([136] is an exception), it is described well in texts on Inverse Problems, eg [20].

For $\mathbf{A} \in \mathbb{C}^{m\times n}$, we recall that $\mathbf{A}^*\mathbf{A}$ is non-negative definite Hermittian so has a complete set of orthogonal eigenvectors $\mathbf{v}_i$ with real eigenvalues $\lambda_1 \geq \lambda_2 \geq \cdots \geq 0$. These are normalized so that $\mathbf{V} = [\mathbf{v}_1 \mid \mathbf{v}_2 \mid \cdots \mid \mathbf{v}_n]$ is a unitary matrix $\mathbf{V}^* = \mathbf{V}^{-1}$. We define $\sigma_i = \sqrt{\lambda_i}$ and for $\sigma_i \neq 0$ $\mathbf{u}_i = {\sigma_i}^{-1}\mathbf{A}\mathbf{v}_i \in \mathbb{C}^m$. Now notice that $\mathbf{A}^*\mathbf{A}\mathbf{v}_i = \lambda_i\mathbf{v}_i = {\sigma_i}^2\mathbf{v}_i$. And $\mathbf{A}^*\mathbf{u}_i = {\sigma_i}^{-1}\mathbf{A}^*\mathbf{A}\mathbf{u}_i = \sigma_i\mathbf{u}_i$. Also $\mathbf{A}\mathbf{A}^*\mathbf{u}_i = {\sigma_i}^2\mathbf{u}_i$, where σ_i are called *singular values*[4] $\mathbf{v}_i$ and $\mathbf{u}_i$ right and left *singular vectors* respectively.

We see that the $\mathbf{u}_i$ are the eigenvectors of the Hermittian matrix $\mathbf{A}\mathbf{A}^*$, so they too are orthogonal. For a non-square matrix $\mathbf{A}$, there are more eigenvectors of either $\mathbf{A}^*\mathbf{A}$ or $\mathbf{A}\mathbf{A}^*$, depending on which is bigger, but only $\min(m, n)$ singular values. If $\operatorname{rank}\mathbf{A} < \min(m, n)$ some of the σ_i will be zero. It is conventional to organize the singular values to be in decreasing order $\sigma_1 \geq \sigma_2 \geq \cdots \geq \sigma_{\min(m,n)} \geq 0$.

If $\operatorname{rank}(\mathbf{A}) = k < n$ then the singular vectors $\mathbf{v}_{k+1}, \ldots, \mathbf{v}_n$ form an orthonormal basis for null $(\mathbf{A})$, whereas $\mathbf{u}_1, \ldots, \mathbf{u}_k$ form a basis for range$(\mathbf{A})$. On the other hand, if $k = \operatorname{rank}(\mathbf{A}) < m$, then $\mathbf{v}_1, \ldots, \mathbf{v}_k$ form a basis for range$(\mathbf{A}^*)$,

[4]The use of σ for singular values is conventional in linear algebra, and should cause no confusion with the use of this symbol for conductivity, which is the accepted symbol for conductivity.

and $\mathbf{u}_{k+1}, \ldots, \mathbf{u}_m$ form an orthonormal basis for null $(\mathbf{A}^*)$. In summary

$$\begin{aligned}
\mathbf{A}\mathbf{v}_i &= \sigma_i \mathbf{u}_i \quad i \leq \min(m,n) \\
\mathbf{A}^*\mathbf{u}_i &= \sigma_i \mathbf{v}_i \quad i \leq \min(m,n) \\
\mathbf{A}\mathbf{v}_i &= 0 \quad \operatorname{rank}(\mathbf{A}) < i \leq n \\
\mathbf{A}^*\mathbf{u}_i &= 0 \quad \operatorname{rank}(\mathbf{A}) < i \leq m \\
\mathbf{u}_i^*\mathbf{u}_j &= \delta_{ij},\ \mathbf{v}_i^*\mathbf{v}_j = \delta_{ij} \\
\sigma_1 &\geq \sigma_2 \geq \cdots \geq 0.
\end{aligned}$$

It is clear from the definition that for any matrix $\mathbf{A}$ $\|\mathbf{A}\| = \sigma_1$ while the Frobenius norm is $\|\mathbf{A}\|_F = \sqrt{\sum_i \sigma_i^2}$. If $\mathbf{A}$ is invertible $\|\mathbf{A}^{-1}\| = 1/\sigma_n$.

The singular value decomposition, SVD, allows us to diagonalize $\mathbf{A}$ using orthogonal transformations. Let $\mathbf{U} = [\mathbf{u}_1 \mid \cdots \mid \mathbf{u}_m]$ then $\mathbf{AV} = \mathbf{U}\Sigma$, where Σ is a the diagonal matrix of singular values padded with zeros to make an $m \times n$ matrix. The nearest thing to diagonalization for non-square $\mathbf{A}$ is

$$\mathbf{U}^*\mathbf{A}\mathbf{V} = \Sigma, \text{ and } \mathbf{A} = \mathbf{U}\Sigma\mathbf{V}^*.$$

Although the SVD is a very important tool for understanding the ill-conditioning of matrices, it is rather expensive to calculate numerically which is prohibitive for large matrices.

In MATLAB the command `s=svd(A)` returns the singular values, `[U,S,V]=svd(A)` gives you the whole singular value decomposition. There are special forms if $\mathbf{A}$ is sparse, or if you only want some of the singular values and vectors.

Once the SVD is known, it can be used to rapidly calculate the Moore-Penrose generalized inverse from

$$\mathbf{A}^\dagger = \mathbf{V}\Sigma^\dagger\mathbf{U}^*$$

where $\Sigma^\dagger$ is simply Σ^T with the non-zero σ_i replaced by $1/\sigma_i$. This formula is valid whatever the rank of $\mathbf{A}$ and gives the minimum norm least squares solution. Similarly the Tikhonov solution is

$$\mathbf{x}_\alpha = \mathbf{V}\mathbf{T}_\alpha\mathbf{U}^*\mathbf{b}$$

where $\mathbf{T}$ is Σ^T with the non-zero σ_i replaced by $\sigma_i/(\sigma_i^2+\alpha^2)$. As only $\mathbf{T}_\alpha$ varies with α one can rapidly recalculate $\mathbf{x}_\alpha$ for a range of α once the SVD is known.

1.4.4 Studying ill-conditioning with the SVD

The singular value decomposition is a valuable tool in studying the ill-conditioning of a problem. Typically we calculate numerically the SVD of a matrix which is a discrete approximation to a continuum problem, and the decay of the singular values gives us an insight into the extent of the instability of the inverse problem. In a simple example [67], calculating k-th derivatives numerically is an illposed problem, in that taking differences of nearby values of a function is

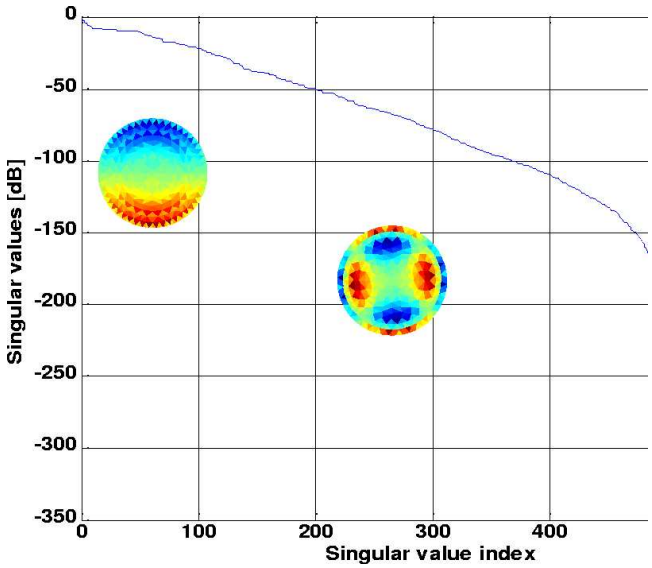

Figure 1.2: Singular values plotted on a logarithmic scale for the linearized 3D EIT problem with ?? electrodes, and some cross sections of two singular vectors.

sensitive to error in the function values. Our operator $\mathbf{A}$ is a discrete version of integrating trigonometric polynomials k-times. The singular vectors of $\mathbf{A}$ are a discrete Fourier basis and the singular value for the i-th frequency proportional to i^{-k}. Problems such as this where $\sigma_i = O(i^{-k})$ for some $k > 0$ are called *mildly illposed*. If we assume sufficient *a priori* smoothness on the function the problem becomes well-posed. By contrast problems such as the inverse Laplace transform, the backward heat equation [67], and linearized EIT the singular values decay faster than any power i^{-k}, and we term them *severely ill-posed*. This degree of ill-posedness technically applies to the continuum problem, but a discrete approximation to the operator will have singular values that approach this behaviour as the accuracy of the approximation increases.

In linearized EIT we can interpret the singular vectors $\mathbf{v}_i$ as telling us that the components $\mathbf{v}_i^*\mathbf{x}$ of a conductivity image $\mathbf{x}$ are increasingly hard to determine as i increases, as they produce voltage changes $\sigma_i \mathbf{u}_i^* x$. With a relative error of ϵ in the data $\mathbf{b}$ we can only expect to reliably recover the components $\mathbf{v}_i^*\mathbf{x}$ of the image when $\sigma_i/\sigma_1 > \epsilon$. A graph of the singular values (for EIT we typically plot σ_i/σ_0 on a logarithmic scale), gives a guide to the number of degrees of freedom in the image we can expect to recover with measurement at a given accuracy. See Figure 1.2.

Another use of the graph of the singular values is determination of rank. Suppose we collect a redundant set of measurements, for example some of the voltages we measure could be determined by reciprocity. As the linear relations between the measurements will transfer to dependencies in the rows of the Ja-

cobian, our if n is greater than the number of independent measurements k, the matrix $\mathbf{A}$ will be rank deficient. In numerical linear algebra linear relations are typically not exact due to rounding error, and rather than having zero singular values we will find that after σ_k the singular values will fall abruptly by several decades. For an example of this in EIT see [23].

The singular values themselves do not tell the whole story. For example two EIT drive configurations may have similar singular values, but if the singular vectors $\mathbf{v}_i$ differ then they will be able to reliably reconstruct different conductivities. To test how easy it is to detect a certain (small as we have linearized) conductivity change $\mathbf{x}$, we look at the singular spectrum $\mathbf{V}^*\mathbf{x}$. If most of the large components are near the top of this vector the change is easy to detect, where as if they are all bellow the l-th row they are invisible with relative error worse than σ_l/σ_0. The singular spectrum $\mathbf{U}^*\mathbf{b}$ of a set of measurements $\mathbf{b}$, gives a guide to how useful that set of measurements will be at a given error level.

1.4.5 More General Regularization

In practical situations the standard Tikhonov regularization is rarely useful unless the variables $\mathbf{x}$ represents coefficients with respect to some well chosen basis for the underlying function. In imaging problems it is natural to take our vector of unknowns as pixel or voxel values, and in EIT one often takes the values of conductivity on each cell (eg triangle or tetrahedron) of some decomposition of the domain, and assumes the conductivity to be constant on that cell. The penalty term $\|\mathbf{x}\|$ in standard Tikhonov prevents extreme values of conductivity but does not enforce smoothness, nor constrain nearby cells to have similar conductivites. As an alternative we choose a positive definite (and without loss of generality Hermittian) matrix $\mathbf{P} \in \mathbb{C}^{n\times n}$ and the norm $\|\mathbf{x}\|_{\mathbf{P}}^2 = \mathbf{x}^*\mathbf{P}\mathbf{x}$. A common choice is to use an approximation to a differential operator $\mathbf{L}$ and set $\mathbf{P} = \mathbf{L}^*\mathbf{L}$.

There are two further refinements which can be included, the first is that we penalise differences from some background value $\mathbf{x}_0$, which can include some known non-smooth behaviour and penalise $\|\mathbf{x} - \mathbf{x}_0\|_{\mathbf{P}}$. The second is to allow for the possibility that we may not wish to fit all measurements to the same accuracy, in particular as some may have larger errors than others. This leads to consideration of the term $\|\mathbf{A}\mathbf{x} - \mathbf{b}\|_{\mathbf{Q}}$ for some diagonal weighting matrix $\mathbf{Q}$. If the errors in $\mathbf{b}$ are correlated, one can consider a non-diagonal $\mathbf{Q}$ so that the errors in $\mathbf{Q}^{1/2}\mathbf{b}$ are not correlated. The probabilistic interpretation of Tikhonov regularization in Box 1.4.5 makes this more explicit. Our Generalized Tikhonov procedure is now

$$\mathbf{x}_{GT} = \arg\min_{\mathbf{x}} \|\mathbf{A}\mathbf{x} - \mathbf{b}\|_{\mathbf{Q}}^2 + \|\mathbf{x} - \mathbf{x}_0\|_{\mathbf{P}}^2.$$

which reduces to the standard Tikhonov procedure for $\mathbf{P} = \mathbf{I}$, $\mathbf{Q} = \alpha^2\mathbf{I}$, $\mathbf{x}_0 = 0$. We can find the solution by noting that for $\tilde{\mathbf{x}} = \mathbf{P}^{1/2}(\mathbf{x}-\mathbf{x}_0)$, $\tilde{\mathbf{A}} = \mathbf{Q}^{1/2}\mathbf{A}\mathbf{P}^{-1/2}$, and $\tilde{b} = \mathbf{Q}^{1/2}(\mathbf{b} - \mathbf{A}\mathbf{x}_0)$

$$\mathbf{x}_{GT} = \mathbf{x}_0 + \mathbf{P}^{-1/2}\arg\min_{\tilde{\mathbf{x}}} \left(\|\tilde{\mathbf{A}}\tilde{\mathbf{x}} - \tilde{\mathbf{b}}\|^2 + \|\tilde{\mathbf{x}}\|^2 \right)$$

which can be written explicitly as

$$\begin{aligned}\mathbf{x}_{GT} &= \mathbf{x}_0 + \mathbf{P}^{-1/2}\left(\tilde{\mathbf{A}}^*\tilde{\mathbf{A}} + \mathbf{I}\right)^{-1}\tilde{\mathbf{A}}^*\tilde{\mathbf{b}} \\ &= \mathbf{x}_0 + \left(\mathbf{A}^*\mathbf{Q}\mathbf{A} + \mathbf{P}\right)^{-1}\mathbf{A}^*\mathbf{Q}(\mathbf{b} - \mathbf{A}\mathbf{x}_0)\end{aligned}$$

or in the alternative forms

$$\begin{aligned}\mathbf{x}_{GT} &= \left(\mathbf{A}^*\mathbf{Q}\mathbf{A} + \mathbf{P}\right)^{-1}\left(\mathbf{A}^*\mathbf{Q}\mathbf{b} + \mathbf{P}\mathbf{x}_0\right) \\ &= \mathbf{x}_0 + \mathbf{P}\mathbf{A}^*\left(\mathbf{A}\mathbf{P}^{-1}\mathbf{A} + \mathbf{Q}^{-1}\right)^{-1}(\mathbf{b} - \mathbf{A}\mathbf{x}_0).\end{aligned}$$

As in the standard Tikhonov case, generalized Tikhonov can be explained in terms of the SVD of $\tilde{\mathbf{A}}$ which can be regarded as the SVD of the operator $\mathbf{A}$ with respect to the $\mathbf{P}$ and $\mathbf{Q}$ norms. Sometimes it is useful to consider a non-invertible $\mathbf{P}$, for example if $\mathbf{L}$ is a first order difference operator $\mathbf{L}^*\mathbf{L}$ has a non-trivial null space. Provided the null space can be expressed as a basis of singular vectors of $\mathbf{A}$ with large σ_i the regularization procedure will still be successful. This situation can be studied using the Generalized Singular Value Decomposition, GSVD [67].

Box 1.3: Probabilistic interpretation of regularization

The statistical approach to regularization [151, Ch 4] gives an alternative justification of generalized Tikhonov regularization. For a detailed treatment of the application of this approach to EIT see [76]. Bayes' theorem relates conditional probabilities of random variables.

$$P(\mathbf{x}|\mathbf{b}) = \frac{P(\mathbf{b}|\mathbf{x})P(\mathbf{x})}{P(\mathbf{b})}.$$

The probability of $\mathbf{x}$ given $\mathbf{b}$ is the probability of $\mathbf{b}$ given $\mathbf{x}$ times $P(\mathbf{x})/P(\mathbf{b})$. We now want the most likely $\mathbf{x}$, so we maximize $P(\mathbf{x}|\mathbf{b})$, the so called Maximum A-Posteriori (MAP) estimate.
This is easy to do if we assume $\mathbf{x}$ is multivariate Gaussian with mean $\mathbf{x}_0$ and covariance $\mathrm{Cov}[\mathbf{x}] = P^{-1}$, and $\mathbf{e}$ has mean zero and $\mathrm{Cov}[\mathbf{e}] = \mathbf{Q}^{-1}$

$$P(\mathbf{x}|\mathbf{b}) = \frac{1}{P(\mathbf{b})}\exp\left(-\frac{1}{2}\|\mathbf{A}\mathbf{x} - \mathbf{b}\|^2_{\mathbf{Q}}\right)\cdot\exp\left(-\frac{1}{2}\|x - x_0\|^2_{\mathbf{P}}\right)$$

where we have used that $\mathbf{x}$ and $\mathbf{e}$ are independent so $P_{\mathbf{b}}(\mathbf{b}|\mathbf{x}) = P_{\mathbf{e}}(\mathbf{b} - \mathbf{A}\mathbf{x})$. We notice that $P(\mathbf{x}|\mathbf{b})$ is maximized by minimizing

$$\|\mathbf{A}\mathbf{x} - \mathbf{b}\|^2_{\mathbf{Q}} + \|\mathbf{x} - \mathbf{x}_0\|^2_{\mathbf{P}}.$$

1.5 Regularizing EIT

We define a forward operator F by $F(\mathbf{s}) = \mathbf{V}$ which takes the vector of degrees of freedom in the conductivity $\mathbf{s}$ to the measured voltages at the boundary $\mathbf{V}$. Clearly F is nonlinear. We will leave aside the adaptive current approach (Section 1.9.3) where the measurements taken depend on the conductivity. As the goal is to fit the actual measured voltages $\mathbf{V}_{\mathrm{m}}$, the simplest approach, as in the case of a linear problem, is to minimize the sum of squares error

$$||\mathbf{V}_{\mathrm{m}} - F(\mathbf{s})||_F^2$$

the so called *output least squares* approach. We have emphasized the Frobenius norm here as $\mathbf{V}_{\mathrm{m}}$ is a matrix, however in this section we will use the notational convenience of using the same symbol when the matrix of measurements is arranged as a column vector. In practice it is not usual to use the raw least squares approach, but at least a weighted sum of squares which reflects the reliability of each voltage. More generally (Box 1.4.5) we use a norm weighted by the inverse of the error covariance. Such approaches are common both in optimization and the statistical approach to inverse problems. To simplify the presentation we will use the standard norm on voltages, or equivalently that they have already been suitably scaled. The more general case is easily deduced from the last section.

Minimization of the voltage error (for simple parameterizations of γ) is doomed to failure as the problem is illposed. In practise the minimum lies in a long narrow valley of the objective function[24]. For a unique solution one must include additional information about the conductivity. An example is to include a penalty $G(\mathbf{s})$ for highly oscillatory conductivites in our minimization, just as in the case of a linear ill-posed problem. We seek to minimize

$$f(\mathbf{s}) = ||\mathbf{V}_m - F(\mathbf{s})||^2 + G(\mathbf{s}).$$

In EIT typical simple choice [146] is

$$G(\mathbf{s}) = \alpha^2 ||\mathbf{L}(\mathbf{s} - \mathbf{s}_{\mathrm{ref}})||^2 \tag{1.10}$$

where $\mathbf{L}$ is a matrix approximation to some partial differential operator and $\mathbf{s}_{\mathrm{ref}}$ a reference conductivity (for example including known anatomical features). The minimization of f represents a trade-off between fitting the data exactly and not making the derivatives of σ too large, the trade off being controlled by the regularisation parameter α.

A common choice [148, 115] is to use a discrete approximation to the Laplacian on piecewise constant functions on the mesh. For each element a sum of the neighboring element values is taken, weighted by the area (or length in 2D) of the shared faces and the total area (perimeter length) of the element multiplied by the element value subtracted. This is analogous to the common five point difference approximation to the Laplacian on a square mesh. Where elements have faces on the boundary, there are no neighbours and the scheme is equivalent to assuming an extension outside the body with the same value. This

enforces a homogeneous Neumann boundary condition so that the null space of $\mathbf{L}$ is just constants. As constant conductivity values are easily obtained in EIT the null space does not diminish the regularizing properties of this choice of G. Similarly one could choose a first order differential operator for $\mathbf{L}$ [143]. Other smooth choices of G include the inverse of a Gaussian smoothing filter [15], effectively an infinite order differential operator. In these cases where G is smooth and for α large enough the Hessian of f will be positive definite, we can then deduce that f is a *convex* function [151, Ch 2], so that a critical point will be a strict local minimum, guaranteeing the success of smooth optimization methods. Such regularization however will prevent us from reconstructing conductivities with a sharp transition, such as an organ boundary. However the advantage of using a smooth objective function f is that it can be minimized using smooth optimization techniques.

Another option is to include in G the *Total Variation*, that is the integral of $|\nabla\gamma|$. This still rules out wild fluctuations in conductivity while allowing step changes. We study this in more detail in Sec 1.6

1.5.1 Linearized Problem

Consider the simplified case is where $F(\mathbf{s})$ is replaced by a linear approximation

$$F(\mathbf{s}_0) + \mathbf{J}(\mathbf{s} - \mathbf{s}_0)$$

where $\mathbf{J}$ is the Jacobian matrix of F calculated at some initial conductivity estimate $\mathbf{s}_0$ (not necessarily the same as $\mathbf{s}_{\text{ref}}$). Defining $\delta\mathbf{s} = \mathbf{s} - \mathbf{s}_0$ and $\delta\mathbf{V} = \mathbf{V}_{\text{m}} - F(\mathbf{s}_0)$ the solution to the linearized regularization problem for the choice of regularization in (1.10) (now a quadratic minimization problem) is given by

$$\delta\mathbf{s} = (\mathbf{J}^*\mathbf{J} + \alpha^2\mathbf{L}^*\mathbf{L})^{-1}(\mathbf{J}^*\delta\mathbf{V} + \alpha^2\mathbf{L}^*\mathbf{L}(\mathbf{s}_{\text{ref}} - \mathbf{s}_0)) \tag{1.11}$$

or any of the equivalent forms [140]. While there are many other forms of regularization possible for a linear ill-conditioned problem this generalised Tikhonov regularization has the benefit that (see Box 1.4.5) the *a priori* information it incorporates is made explicit and that under Gaussian assumptions it is the statistically defensible MAP estimate. If only a linearised solution to be used with a fixed initial estimate $\mathbf{s}_0$ the Jacobian $\mathbf{J}$ and a factorization of $(\mathbf{J}^*\mathbf{J} + +\alpha^2\mathbf{L}^*\mathbf{L})$ can be precalculated off-line. The efficiency of this calculation is then immaterial and the regularized solution can be calculated using the factorization with complexity $O(N^2)$ for N degrees of freedom in the conductivity (which should be smaller than the number of independent measurements). Although LU factorization would be one alternative, perhaps a better choice is to use the Generalized Singular Value Decomposition GSVD [67], which allows the regularized solution to be calculated efficiently for any value of α. The GSVD is now a standard tool for understanding the effect of the choice of the regularization matrix $\mathbf{L}$ in a linear ill-conditioned problem, and has been applied to linearized EIT[143, 15]. The use of a single linearized Tikhonov regularized solution is widespread in medical industrial and geophysical EIT, the NOSER algorithm [32] being a well known example.

1.5.2 Backprojection

It is an interesting historical observation that in the medical and industrial applications of EIT numerous authors have calculated $\mathbf{J}$ and then proceeded to use *ad hoc* regularized inversion methods to calculate an approximate solution. Often these are variations on standard iterative methods which, if continued would for a well posed problem converge to the Moore-Penrose generalised solution. It is a standard method in inverse problems to use an iterative method but stop short of convergence (Morozov's discrepancy principle tells us to stop when the output error first falls below the measurement noise). Many linear iterative schemes can be represented as a filter on the singular values. However the have the weakness that the *a priori* information included is not as explicit as in Tikhonov regularisation. One extreme example of the use of an *ad hoc* method is the method described by Kotre [83] in which the normalized transpose of the Jacobian is applied to the voltage difference data. In the Radon transform used in X-Ray CT [107], the formal adjoint of the Radon transform is called the *back projection* operator. It produces at a point in the domain the sum of all the values measured along rays through that point. Although not an inverse to the Radon transform itself, a smooth image can be obtained by back-projecting smoothed data, or equivalently by back-projecting then smoothing the resulting image.

The Tikhonov regularization formula (1.11) can be interpreted in a loose way as the back-projection operator $\mathbf{J}^*$ followed be application of the spatial filter $(\mathbf{J}^*\mathbf{J} + +\alpha^2\mathbf{L}^*\mathbf{L})^{-1}$. Although this approach is quite different from the filtered back projection along equipotential lines of Barber and Brown [8, 123] it is sometimes confused with this in the literature. Kotre's back projection was until recently widely used in the process tomography community for both resistivity (ERT) and permittivity (ECT) imaging [154]. Often supported by the fallacious arguments, in particular that it is fast (it is no faster than the application of any precomputed regularized inverse) and that it is commonly used (only by those who know no better). In an interesting development the application of a normalised adjoint to the residual voltage error for the linearised problem was suggested for ECT, and later recognised as yet another reinvention of the well known Landweber iterative method [153]. Although there is no good reason to use pure linear iteration schemes directly on problems with such small a number of parameters as they can be applied much faster using the SVD, an interesting variation is to use such a slowly converging linear solution together with projection on to a constraint set. A method which has been shown to work well in ECT [27].

1.5.3 Iterative Nonlinear Solution

The use of linear approximation is only valid for small deviations from the reference conductivity. In medical problems conductivity contrasts can be large, but there is a good case for using the linearized method to calculate a change in admittivity between two states, measured either at different times or with

different frequencies. Although this has been called "dynamic imaging" in EIT the term *difference imaging* is now preferred (*dynamic imaging* is a better used to describe statistical time series method such as [145]). In industrial ECT modest variations of permittivity are commonplace. In industrial problems and in phantom tanks it is possible to measure a reference data set using a homogeneous tank. This can be used to calibrate the forward model, in particular the contact impedance can be estimated [69]. In an *in vivo* measurement there is no such possibility and it may be that the mismatch between the measured data and the predictions from the forward model is dominated by the errors in electrode position, boundary shape and contact impedance rather than interior conductivity. Until these problems are overcome it is unlikely, in the author's opinion, to be worth using iterative non-linear methods *in vivo* using individual surface electrodes. Note however that such methods are in routine use in geophysical problems [89, 90].

The essence of non-linear solution methods is to repeat the process of calculating the Jacobian and solving a regularised linear approximation. However a common way to explain this is to start with the problem of minimizing f, which for a well chosen G will have a critical point which is the minimum. At this minimum $\nabla f(\mathbf{s}) = \mathbf{0}$ which is a system of N equations in N unknowns which can be solved by multi-variable Newton-Raphson method. The Gauss-Newton approximation to this, which neglects terms involving second derivatives of F, is a familiar Tikhonov formula updating the n th approximation to the conductivity parameters $\mathbf{s}_n$

$$\mathbf{s}_{n+1} = \mathbf{s}_n + (\mathbf{J}_n^* \mathbf{J}_n + \alpha^2 \mathbf{L}^* \mathbf{L})^{-1} (\mathbf{J}_n^* (\mathbf{V}_{\mathrm{m}} - F(\mathbf{s}_n)) + \alpha^2 \mathbf{L}^* \mathbf{L} (\mathbf{s}_{\mathrm{ref}} - \mathbf{s}_n)$$

where $\mathbf{J}_n$ is the Jacobian evaluated at $\mathbf{s}_n$, and care has to be taken with signs . Notice that in this formula the Tikhonov parameter is held constant throughout the iteration, by contrast the Levenberg-Marquardt[104] method applied to $\nabla f = 0$ would add a diagonal matrix λD in addition to the regularization term $\alpha^2 L^* L$ but would reduce λ to zero as a solution was approached. For an interpretation of λ as a Lagrangian multiplier for an optimization constrained by a *trust region* see [151, Ch 3]. Another variation on this family of methods is, given an update direction from the Tikhonov formula, to do an approximate *line search* to minimize f in that direction. Both methods are described in [151, Ch 3].

The parameterization of the conductivity can be much more specific than voxel values or coefficients of smooth basis functions. One example is to assume that the conductivity is piecewise constant on smooth domains and reconstruct the shapes parameterized by Fourier series [68, 77, 80, 81] or by level sets [122, 44, 31, 36]. For this and other model based approaches the same family of smooth optimization techniques can be used as for simpler parameterizations, although the Jacobian calculation may be more involved. For inclusions of known conductivities there are a range of direct techniques we will briefly survey in Sec 1.12.2.

1.6 Total Variation Regularization

The Total Variation functional is assuming an important role in the regularisation of inverse problems belonging to many disciplines, after its first introduction by Rudin, Osher and Fatemi (1992) [120] in the image restoration context. The use of such a functional as a regularisation penalty term allows the reconstruction of discontinuous profiles. As this is a desirable property, the method is gaining popularity.

Total variation measures the total amplitude of the oscillations of a function. For a differentiable function on a domain Ω the total variation is [43]

$$TV(f) = \int_{\Omega} |\nabla f| \tag{1.12}$$

The definition can be extended to non–differentiable functions [57] as:

$$TV(f) = \sup_{\mathbf{v}\in\mathcal{V}} \int_{\Omega} f \ \mathrm{div}\, \mathbf{v} \tag{1.13}$$

where $\mathcal{V}$ is the space of continuously differentiable functions that vanish on $\partial\Omega$ and $\|\mathbf{v}\|_{\Omega} \leq 1$.

As the TV functional measures the variations of a function over its domain, it can be understood to be effective at reducing oscillations in the inverted profile, if used as a penalty term. The same properties apply however to ℓ_2 regularisation functionals. The important difference is that the class of functions with bounded total variation also includes discontinuous functions, which makes the TV particularly attractive for the regularisation of non–smooth profiles. The following one-dimensional example illustrates the advantage of using the TV against a quadratic functional in non-smooth contexts

Let $F = \{f : [0,1] \to \mathbb{R}, |\, f(0) = a, f(1) = b\}$, we have

- $\min\limits_{f\in F} \int_0^1 |f'(x)|\mathrm{d}x$ is achieved by any monotonic function, including discontinuous ones.
- $\min\limits_{f\in F} \int_0^1 (f'(x))^2\mathrm{d}x$ is achieved only by the straight line connecting the points $(0,a)\,(1,b)$.

Figure 1.3 shows three possible functions f_1, f_2, f_3 in F. All of them have the same total variation, including f_3 which is discontinuous. Only f_2 however minimises the H^1 semi–norm

$$|f|_{H_1} = \left(\int_0^1 \left(\frac{\partial f}{\partial x} \right)^2 \mathrm{d}x \right)^{1/2}. \tag{1.14}$$

The quadratic functional, if used as penalty, would therefore bias the inversion toward the linear solution and the function f_3 would not be admitted in the solution set as its H^1 semi-norm is infinite.

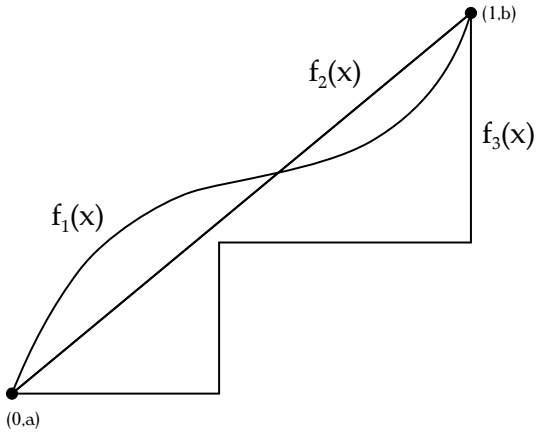

Figure 1.3: Three possible functions: $f_1, f_2, f_3 \in F$. All of them have the same TV, but only f_2 minimises the H^1 semi-norm.

Two different approaches proposed for application of TV to EIT, the first by Dobson *et. al.* [60] and the second by Somersalo *et. al.* and Kolehmainen *et. al.* [132] [82]. The approach proposed by Dobson and Santosa is suitable for the linearised problem and suffers from poor numerical efficiency. Somersalo and Kolehmainen successfully applied MCMC methods to solve the TV regularised inverse problem. The advantage in applying MCMC methods over deterministic methods is that they do not suffer from the numerical problems involved with non-differentiability of the TV functional. They do not require *ad hoc* techniques. Probabilistic methods, such as MCMC, offer central estimates and errors bars by sampling the posterior probability density of the sought parameters. The sampling process involves a substantial computational effort, often the inverse problem is linearised in order to speed up the sampling. What is required is an efficient method for deterministic Tikhonov style regularisation, to offer a non–linear TV regularised inversion in a short time. We will briefly describe the Primal Dual Interior Point Method (PD-IPM) to TV applied to EIT [14, 13] which is just such a method. In Sec 1.10 we present some numerical results using this method for the first time for 3D EIT.

A second aspect, which adds importance to the study of efficient MAP (Tikhonov) methods, is that the linearisation in MCMC methods is usually performed after an initial MAP guess. Kolehmainen [82] reports calculating several iterations of a Newton method before starting the burn-in phase of his algorithm. A good initial deterministic TV inversion could therefore bring benefit to these approaches.

Examining the relevant literature, a variety of deterministic numerical methods have been used for the regularisation of image denoising and restoration problems with the TV functional (a good review is offered by Vogel in [151]). The numerical efficiency and stability are the main issues to be addressed. Use

of *ad–hoc* techniques is common, given the poor performance of traditional algorithms. Most of the deterministic methods draw from ongoing research in optimisation, as TV minimisation belongs to the important classes of problems known as "Minimisation of sum of norms" [38] [3] [4] and "Linear ℓ_1 problems" [10] [156].

1.6.1 Duality for Tikhonov Regularised Inverse Problems

In inverse problems, with linear forward operators, the discretised TV regularised inverse problem, can be formulated as

$$(P) \quad \min_{\mathbf{x}} \frac{1}{2}\|\mathbf{A}\mathbf{x} - \mathbf{b}\|^2 + \alpha\|\mathbf{L}\,\mathbf{x}\| \tag{1.15}$$

where **L**is a discretization of the gradient operator. We will label it as the primal problem. A *Dual* problem to (P), which can be shown to be equivalent [13] is

$$(D) \quad \max_{\mathbf{y}:\|\mathbf{y}\|\leq 1} \quad \min_{\mathbf{x}} \frac{1}{2}\|\mathbf{A}\mathbf{x} - \mathbf{b}\|^2 + \alpha\,\mathbf{y}^T\mathbf{L}\mathbf{x} \tag{1.16}$$

The optimisation problem

$$\min_{\mathbf{x}} \frac{1}{2}\|\mathbf{A}\mathbf{x} - \mathbf{b}\|^2 + \alpha\,\mathbf{y}^T\mathbf{L}\mathbf{x} \tag{1.17}$$

has an optimal point defined by the first order conditions

$$\mathbf{A}^T(\mathbf{A}\mathbf{x} - \mathbf{b}) + \alpha\,\mathbf{L}^T\mathbf{x} = 0 \tag{1.18}$$

the dual problem can be written therefore as

$$(D) \qquad \begin{aligned} \max_{\mathbf{y}\,:\,\|\mathbf{y}\|\leq 1} \quad & \frac{1}{2}\|\mathbf{A}\mathbf{x} - \mathbf{b}\|^2 + \alpha\,\mathbf{y}^T\mathbf{L}\mathbf{x} \\ A^T(A\mathbf{x} - \mathbf{b}) + \alpha\,L^T\mathbf{y} &= 0 \end{aligned} \tag{1.19}$$

The complementarity condition for (1.15) and (1.19) is set by nulling the primal dual gap

$$\frac{1}{2}\|\mathbf{A}\mathbf{x} - \mathbf{b}\|^2 + \alpha\,\|L\,\mathbf{x}\| - \frac{1}{2}\|A\mathbf{x} - \mathbf{b}\|^2 - \alpha\mathbf{y}^T\mathbf{L}\mathbf{x} = 0 \tag{1.20}$$

which with the dual feasibility $\|\mathbf{y}\| \leq 1$ is equivalent to requiring that

$$\mathbf{L}\mathbf{x} - \|\mathbf{L}\mathbf{x}\|\mathbf{y} = 0 \tag{1.21}$$

The PD-IPM framework for the TV regularised inverse problem can thus be written as

$$\|\mathbf{y}\| \leq 1 \tag{1.22a}$$

$$\mathbf{A}^T(\mathbf{A}\mathbf{x} - \mathbf{b}) + \alpha\,L^T\mathbf{y} = 0 \tag{1.22b}$$

$$\mathbf{L}\mathbf{x} - \|\mathbf{L}\mathbf{x}\|\mathbf{y} = 0 \tag{1.22c}$$

It is not possible to apply the Newton Method directly to (1.22) as (1.22c) is not differentiable for $\mathbf{L}\mathbf{x} = 0$. A centering condition has to be applied, obtaining a smooth pair of optimisation problems (P_β) and (D_β) and a central path parameterised by β. This is done by replacing $\|\mathbf{L}\mathbf{x}\|$ by $(\|\mathbf{L}\mathbf{x}\|^2 + \beta)^{\frac{1}{2}}$ in (1.22c).

1.6.2 Application to EIT

The PD-IPM algorithm in its original form [30] was developed for inverse problems with linear forward operators. The following section (based on [13]) describes the numerical implementation for EIT reconstruction. The implementation is based on the results of the duality theory for inverse problems with linear forward operators. Nevertheless it was possible to apply the original algorithm to the EIT inverse problem with minor modifications, and to obtain successful reconstructions. The formulation for the EIT inverse problem is

$$\begin{array}{c} \mathbf{s}_{rec} = \arg\,\min_{\mathbf{s}} f(\mathbf{s}) \\ f(\mathbf{s}) = \frac{1}{2}\|F(\mathbf{s}) - \mathbf{V}_{\mathrm{m}}\|^2 + \alpha\, TV(\mathbf{s}) \end{array} \tag{1.23}$$

With a similar notation as used in Section 1.6.1, the system of non–linear equations that defines the PD–IPM method for (1.23) can be written as

$$\begin{array}{c} \|\mathbf{y}\| \leq 1 \\ J^T(F(\mathbf{s}) - \mathbf{V}_{\mathrm{m}}) + \alpha\, L^T\mathbf{y} = 0 \\ L\mathbf{s} - E\mathbf{y} = 0 \end{array} \tag{1.24}$$

with $E = \sqrt{\|\mathbf{L}\,\mathbf{s}\|^2 + \beta}$, and J the Jacobian of the forward operator $F(\mathbf{s})$. Newton's method can be applied to solve (1.24) obtaining the following system for the updates $\delta\mathbf{s}$ and $\delta\mathbf{y}$ of the primal and dual variables

$$\left[\begin{array}{cc} J^TJ & \alpha\, L^T \\ EL & -E \end{array}\right] \left[\begin{array}{c} \delta\mathbf{s} \\ \delta\mathbf{y} \end{array}\right] = -\left[\begin{array}{c} J^T(F(\mathbf{s}) - \mathbf{b}) + \alpha\, L^T\mathbf{y} \\ L\mathbf{s} - E\mathbf{y} \end{array}\right] \tag{1.25}$$

with

$$h = 1 - \frac{\mathbf{y}\mathbf{L}\,\mathbf{s}}{E} \tag{1.26}$$

which in turn can be solved as follows

$$[J^TJ + \alpha\, L^TE^{-1}hL]\,\delta\mathbf{s} = -[J^T(F(\mathbf{s}) - \mathbf{b}) + \alpha\, L^TE^{-1}L\,\mathbf{s}] \tag{1.27a}$$

$$\delta\mathbf{y} = -\mathbf{y} + E^{-1}L\mathbf{s} + E^{-1}hL\,\delta\mathbf{s} \tag{1.27b}$$

Equations (1.27) can therefore be applied iteratively to solve the non–linear inversion (1.23). Some care must be taken on the dual variable update, to maintain dual feasibility. A traditional line search procedure with feasibility checks is not suitable as the dual update direction is not guaranteed to be an ascent direction for the penalised dual objective function (D_β). The simplest way to compute the update is called the *scaling rule* [4] which is defined to work as follows

$$\mathbf{y}_{k+1} = \lambda(\mathbf{y}_k + \delta\mathbf{y}_k) \tag{1.28}$$

where

$$\lambda = \max\{\lambda :\ \lambda\|\mathbf{y}_k + \delta\mathbf{y}_k\| \leq 1\} \tag{1.29}$$

An alternative way is to calculate the exact step length to the boundary, applying what is called the *steplength rule* [4]

$$\mathbf{y}_{k+1} = \mathbf{y}_k + \min(1, \lambda)\,\delta\mathbf{y}_k \tag{1.30}$$

where

$$\lambda = \max\{\lambda : \ \|\mathbf{y}_k + \lambda\, \delta\mathbf{y}_k\| \leq 1\} \tag{1.31}$$

In the context of EIT, and in tomography in general, the computation involved in calculating the exact step length to the boundary of the dual feasibility region is negligible compared to the whole algorithm iteration. It is convenient therefore to adopt the exact update, which in our experiments resulted in a better convergence. The scaling rule has the further disadvantage of always placing $\mathbf{y}$ on the boundary of the feasible region, which prevents the algorithm from following the central path. Concerning the updates on the primal variable, the update direction $\delta\mathbf{s}$ is a descent direction for (P_β) therefore a line search procedure could be opportune. In our numerical experiments we have found that for relatively small contrasts (e.g. 3:1) the primal line search procedure is not needed, as the steps are unitary. For larger contrasts a line search on the primal variable guarantees the stability of the algorithm.

1.7 Jacobian calculations

In optimization based methods it is often necessary to calculate the derivative of the voltage measurements with respect to a conductivity parameter. The complete matrix of partial derivatives of voltages with respect to conductivity parameters is the *Jacobian* matrix, sometimes in the medical and industrial EIT literature called the *sensitivity matrix*, or the rows are called *sensitivity maps*. We will describe here the basic method for calculating this efficiently with a minimal number of forward solutions. Let is be said first that there are methods where the derivative is calculated only once and although the forward solution is calculated repeatedly as the conductivity is updated. This is the difference between *Newton-Kantorovich* method and Newton's method. There are also *Quasi-Newton* methods in which the Jacobian is update approximately from the forward solutions that have been made. Indeed this has been used in geophysics [90]. It also worth pointing out that were the conductivity is parameterized in a non-linear way for example using shapes of an anatomical model, that the Jacobian with respect to those new parameters can be calculated using the chain rule.

1.7.1 Perturbation in power

Using the weak form of $\nabla \cdot \gamma\nabla\phi = 0$ (or Green's identity), for any w

$$\int_\Omega \gamma\nabla\phi \cdot \nabla w \, dV = \int_{\partial\Omega} w\gamma \frac{\partial\phi}{\partial n}\, dS \tag{1.32}$$

We use the complete electrode model. For the special case $w = \bar{\phi}$ we have the power conservation formula,

$$\int_\Omega \gamma|\nabla\phi|^2 \, dV = \int_{\partial\Omega} \overline{\phi}\, \gamma \frac{\partial\phi}{\partial n}\, dS = \sum_l \int_{E_l} \overline{\left(V_l - z_l\gamma\frac{\partial\phi}{\partial n}\right)}\gamma\frac{\partial\phi}{\partial n}\, dS \tag{1.33}$$

hence

$$\int_\Omega \gamma|\nabla\phi|^2\,dV + \sum_l \int_{E_l} \overline{z_l}\left|\gamma\frac{\partial\phi}{\partial n}\right|^2 = \sum_l \overline{V_l}I_l \tag{1.34}$$

This simply states that the power input is dissipated either in the domain Ω or by the contact impedance layer under the electrodes.

In the case of full time harmonic Maxwell's equations (Box 1.2) the power flux is given by the Poynting vector $\mathbf{E}\times\mathbf{H}$ the complex power crossing the boundary is then equal to the complex power dissipated and stored in the interior (the imaginary part representing the power stored as electric and magnetic energy)

$$\int_{\partial\Omega} \mathbf{E}\times\mathbf{H}\cdot\mathbf{n} = \int_\Omega \gamma\mathbf{E}\cdot\mathbf{E} + \imath\omega\mathbf{H}\cdot\mathbf{H} \tag{1.35}$$

which generalizes (1.34).

1.7.2 Standard formula for Jacobian

We now take perturbations $\gamma\to\gamma+\delta\gamma$, $\phi\to\phi+\delta\phi$ and $V_l\to V_l+\delta V_l$, with the current in each electrode I_l held constant. We calculate the first order perturbation, and argue as in [28, 26] that the terms we have neglected are higher order in the L^∞ norm on $\delta\gamma$. The details of the calculation are given for the complete electrode model case in [115], the result is

$$\sum_l \overline{I_l}\delta V_l = -\int_\Omega \delta\gamma|\nabla\phi|^2\,dV \tag{1.36}$$

This gives only the total change in power, to get the change in voltage on a particular electrode E_m when a current pattern is driven in some or all of the other electrodes we simply solve for the special 'measurement current pattern' $\widetilde{I}_l^m=\delta_{lm}$. To emphasize the dependence of the potential on a vector of electrode currents $\mathbf{I}=(I_1,\ldots,I_L)$ we write $\phi(\mathbf{I})$. The hypothetical measurement potential is $u(\mathbf{I}^m)$, by contrast the potential for the d-th drive pattern $\phi(\mathbf{I}^d)$. Applying the power perturbation formula (1.36) to $\phi(\mathbf{I}^d)+\overline{\phi(\mathbf{I}^m)}$ and $\phi(\mathbf{I}^d)-\overline{\phi(\mathbf{I}^m)}$ and then subtracting gives the familiar formula

$$\delta V_{dm} = -\int_\Omega \delta\gamma\nabla\phi(\mathbf{I}^d)\cdot\nabla\phi(\mathbf{I}^m)\,dV \tag{1.37}$$

While this formula gives the Fréchet derivative for $\delta\gamma\in L^\infty(\Omega)$, considerable care is needed to show that the voltage data is Fréchet differentiable in other norms, such as those needed to show that the total variation regularization scheme works [152]. For a finite dimensional subspace of $L^\infty(\Omega)$ a proof of differentiability is given in [76].

For full time harmonic Maxwell's equations the power conservation formula (1.35) yields a sensitivity to a perturbation of admittivity exactly as in (1.37) but the electric field $\mathbf{E}$ is no longer a gradient and sensitivity to a change in the magnetic permeability is given by $\mathbf{H}\cdot\mathbf{H}$ [131]

In the special case of the Sheffield adjacent pair drive, adjacent pair measurement protocol we have potentials ϕ_i for the i-th drive pair and voltage measurement V_{ij} for a constant current I

$$\delta V_{ij} = -\frac{1}{I^2} \int_\Omega \delta\gamma \nabla\phi_i \cdot \overline{\nabla\phi_j}\, dV \tag{1.38}$$

To calculate the Jacobian matrix one must choose a discretizarion of the conductivity. The simplest case is to take the conductivity to be piecewise constant on polyhedral domains such as voxels or tetrahedral elements. Taking $\delta\gamma$ to be the characteristic function of the k-th voxel Ω_k we have for a fixed current pattern

$$J_{dm\,k} = \frac{\partial V_{dm}}{\partial \gamma_k} = -\int_{\Omega_k} \nabla u(\mathbf{I}^d) \cdot \nabla\overline{\phi(\mathbf{I}^m)}\, dV \tag{1.39}$$

Some EIT and capacitance tomography systems use a constant voltage source and in this case the change in power of an increase in admittivity will have the opposite sign to the constant current case.

A common variation in the case of real conductivity is to use the resistivity $\rho = 1/\sigma$ as the primary variable or more commonly to use $\log\sigma$ [9, 24, 146], which has the advantage that it does not need to be constrained to be positive. With a simple parameterization of conductivity as constant on voxels $g(\gamma)$ is constant on voxels as well. In this case from the chain rule we simply use the chain rule, dividing the k-th column of Jacobian we have calculated by $g'(\gamma_k)$. The regularization will also be affected by the change of variables.

Box 1.4: Sensitivity to a localised change in conductivity

Studying the change in voltage from a small localised change in conductivity is a useful illustration of EIT. Suppose we fix a current pattern, and a background conductivity of γ, which results in a potential ϕ. Now consider a perturbed conductivity $\gamma + \delta\gamma$ which results in a potential, with the same current drive, $\phi + \delta\phi$. From $\nabla \cdot (\gamma + \delta\gamma)\nabla\phi = 0$ we see that

$$\nabla \cdot \delta\gamma\nabla\phi + \nabla \cdot \gamma\nabla\delta\phi + \nabla \cdot \delta\gamma\nabla\delta\phi = 0$$

The same procedure used to calculate the Jacobian can be used to show that the last term is $O(\delta\gamma^2)$ so that to first order

$$\nabla \cdot \gamma\nabla\delta\phi = -\nabla \cdot \delta\gamma\nabla\phi$$

now for simplicity take $\gamma = 1$ and we have the Poisson equation for $\delta\phi$

$$\nabla^2\delta\phi = \nabla\delta\gamma \cdot \nabla\phi$$

If we now take $\delta\gamma$ to be a small change constant on a small ball near some point p, then the source term in this Poisson equation approximates a dipole at p whose strength and direction is given by $\nabla\phi$. Observing $\delta\phi$ at the boundary we see it as a dipole field from which a line through p can be estimated by eye. This goes some way to explain the ease with which one small object can be located, even with only a small number of current patterns. It also illustrates the depth dependence of the sensitivity as the dipole field decays with distance even if the electric field is relatively uniform. Typically the electric field strength is also less away from the boundary.
This continuum argument is paralleled in Yorkey's 'compensation' method in resistor networks [155]. A resistor in a network is changed and Yorkey observes that to first order the change in voltage at each point in the network is equivalent to the voltage which would result if a current source were applied in parallel with that resistor.

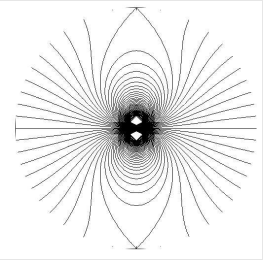

The potential due to a dipole source at the centre of a homogeneous disk

Some iterative nonlinear reconstruction algorithms, such as nonlinear Landwe-

ber, or non-linear conjugate gradient (see Sec 1.8.3 and [151]) require the evaluation of transpose (or adjoint) of the Jacobian multiplied by a vector $\mathbf{J}^* z$. For problems where the Jacobian is very large it may be undesirable to store the Jacobian and then apply its transpose to z. Instead the block of z_i corresponding to the ith current drive is written as distributed source on the measurement electrodes. A forward solution is performed with this as the boundary current pattern so that when this measurement field is combined with the field for the drive pattern as 1.39, and this block accumulated to give $\mathbf{J}^* z$. For details of this applied to diffuse optical tomography see [5], and for a general theory of adjoint sources see [151]

For fast calculation of the Jacobian using (1.39) one can precompute the integrals of products of finite element basis functions over elements. If non constant basis functions are used on elements, or higher order elements used one could calculate the product of gradients of FE basis functions at quadrature points in each element. As this depends only on the geometry of the mesh and not the conductivity this can be precomputed unless one is using an adaptive meshing strategy. The same data is used in assembling the FE system matrix efficiently when the conductivity has changed but not the geometry. It is these factors particularly which make current commercial FEM software unsuitable for use in an efficient EIT solver.

1.8 Solving the forward problem: the Finite Element Method

In addition to the close integration of the Jacobian calculation and the FEM forward solver, another factor which leads those working on EIT reconstruction to write their own FEM program that the Complete Electrode Model is a non-standard type of boundary condition not included in commercial FEM software. It is not hard to implement and there are freely available codes [148, 115], but it is worth covering the basic theory here for completeness. A good introduction to FEM in electromagnetics is [129], and details of implementation of the CEM can be found especially in the theses [146, 116].

1.8.1 Basic FEM formulation

Our starting point is to approximate the domain Ω as union of a finite number of cells, which for simplicity we will take to be *simplices*. In two dimensions a simplex is a triangle and in three dimensions a tetrahedron. More generally quadrilaterals, hexahedra and prisms can be used. The cells must arranged so that they intersect only on whole faces. A collection of such simplices is called a Finite Element mesh, and we will suppose that there are K simplices with N vertices. We will approximate the potential using this mesh by functions which are linear on each simplex, and continuous across the faces. These functions have the appealing feature that they are completely determined by their values at the vertices. A natural basis is the set of functions v_i which are one on

vertex i and zero at the other vertices and we can represent the potential by the approximation

$$\phi_{\mathrm{FEM}}(\mathbf{x}) = \sum_{i=1}^{N} \phi_i w_i(\mathbf{x}). \tag{1.40}$$

so that $\Phi = (\phi_1, \ldots, \phi_n)^T \in \mathbb{C}^N$ is vector which represents our discrete approximation to the potential.

As our basis functions w_i are not differentiable we cannot directly satisfy (1.1). Instead we drive the weak form of the equation. Multiplying (1.1) by some function v and integrating over Ω,

$$\int_\Omega v\, \nabla \cdot (\gamma \nabla \phi)\, dV = 0 \qquad \text{in } \Omega \tag{1.41}$$

and we demand that this vanishes for all functions v is a certain class. Clearly this is weaker than assuming directly that $\nabla \cdot (\gamma \nabla \phi) = 0$.

Using Green's second identity and the vector identity

$$\nabla \cdot (v\, \gamma \nabla \phi) = \gamma \nabla \phi \cdot \nabla v + v \nabla \cdot (\gamma \nabla \phi) \tag{1.42}$$

the equation (1.41) is changed to

$$\int_\Omega \nabla \cdot (v\, \gamma \nabla \phi)\, dV - \int_\Omega \gamma \nabla \phi \cdot \nabla v\, dV = 0 \tag{1.43}$$

Invoking the divergence theorem

$$\int_\Omega \nabla \cdot (v\, \gamma \nabla \phi)\, dV = \int_{\partial\Omega} v\, \gamma \nabla \phi \cdot \mathbf{n} dS \tag{1.44}$$

gives

$$\begin{aligned} \int_\Omega \gamma\, \nabla \phi \cdot \nabla v\, dV &= \int_{\partial\Omega} \gamma \nabla \phi \cdot \mathbf{n}\, v\, dS \\ &= \int_\Gamma \gamma \nabla \phi \cdot \mathbf{n}\, v\, dS \end{aligned} \tag{1.45}$$

where $\Gamma = \bigcup_l E_l$ is the union of the electrodes, and we have used the fact that the current density is zero off the electrodes. For a given set of test functions v (1.45) is the weak formulation of the boundary value problem for 1.1 with current density specified on the electrodes.

Rearranging the boundary condition (1.6) as

$$\gamma \nabla \phi \cdot \mathbf{n} = \frac{1}{z_l}(V_l - \phi) \tag{1.46}$$

on E_l for $z_l \neq 0$ and incorporating it into (1.45) gives

$$\int_\Omega \gamma \nabla \phi \cdot \nabla v\, dV = \sum_{l=1}^{L} \int_{E_l} \frac{1}{z_l}(V_l - \phi)\, v\, dS \tag{1.47}$$

In the finite element method we use test functions in the same family we use to approximate potentials $v = \sum_{i=0}^{N} v_i w_i$, substitution of this and ϕ_{FEM} for ϕ gives for each i

$$\sum_{j=1}^{N}\left\{\int_{\Omega}\gamma\nabla w_i\cdot\nabla w_j\,dV\right\}\phi_j+\sum_{l=1}^{L}\int_{E_l}\frac{1}{z_l}w_i w_j\,dS\Big\}\phi_j-\sum_{l=1}^{L}\left\{\int_{E_l}\frac{1}{z_l}w_i\,dS\right\}V_l=0 \tag{1.48}$$

Together with the known total current

$$\begin{aligned} I_l &= \int_{E_l}\frac{1}{z_l}(V_l-\phi)\,dS \\ &= \int_{E_l}\frac{1}{z_l}V_l-\sum_{i}^{N}\left\{\int_{E_l}\frac{1}{z_l}w_i\,dS\right\}\phi_i \end{aligned} \tag{1.49}$$

and if we assume z_l is constant on E_l this reduces to

$$I_l=\frac{1}{z_l}|E_l|V_l-\frac{1}{z_l}\sum_{i}^{N}\left\{\int_{E_l}w_i\,dS\right\}\phi_i \tag{1.50}$$

where $|E_l|$ is the area (or in 2D length) of the l-th electrode.

We now need to choose how to approximate γ, and a simple method is to choose γ to be constant on each simplex (piece-wise constant). The characteristic function χ_j is one on the j-th simplex and zero elsewhere so we have an approximation to γ

$$\gamma_{\text{PWC}}=\sum_{j=1}^{k}\gamma_j\chi^j \tag{1.51}$$

which has the advantage that the γ_j can be taken outside of an integral over each simplex. If a more elaborate choice of basis is used it would be wise to use a higher order quadrature rule.

Our FE system equations now take the form

$$\begin{bmatrix} A_M+A_Z & A_W \\ A_W^T & A_D \end{bmatrix}\begin{bmatrix}\Phi\\ V\end{bmatrix}=\begin{bmatrix}0\\ I\end{bmatrix} \tag{1.52}$$

were A_M is an $N\times N$ symmetric matrix

$$\begin{aligned} A_{M\,ij} &= \int_{\Omega}\gamma\nabla w_i\cdot \\ &= \sum_{k=1}^{K}\gamma_k\int_{\Omega_k}\nabla w_i\nabla w_j\,dV \end{aligned} \tag{1.53}$$

which is the usual system matrix for (1.1) without boundary conditions, while

$$A_{Z\,ij}=\sum_{l=1}^{L}\int_{E_l}\frac{1}{z_l}w_i w_j\,dS, \tag{1.54}$$

$$A_{W\,li} = -\frac{1}{z_l}\int_{E_l} w_i \, dS, \tag{1.55}$$

and

$$A_D = \operatorname{diag}\left(\frac{|E_l|}{z_l}\right) \tag{1.56}$$

implement the CEM boundary conditions. One additional constraint is required as potentials are only defined up to an added constant. One elegant choice is to change the basis used for the vectors V and I to a basis for the subspace S orthogonal to constants, for example the vectors

$$\left[\tfrac{1}{L-1}, \ldots, \tfrac{1}{L-1}, 1, \tfrac{1}{L-1}, \ldots, \tfrac{1}{L-1}\right]^T. \tag{1.57}$$

while another choice is to 'ground' an arbitrary vertex i by setting $\phi_i = 0$. The resulting solution Φ can then have any constant added to produce a different grounded point.

As the contact impedance decreases the system (1.52) becomes ill-conditioned. In this case (1.6) in the CEM can be replaced by the *shunt model* which simply means the potential ϕ is constrained to be constant on each electrode. This constraint can be enforced directly replacing all nodal voltages on electrode E_l by one unknown V_l.

It is important for EIT to notice that the conductivity only enters in the system matrix as linear multipliers of

$$s_{ijk} = \int_{\Omega_k} \nabla w_i \cdot \nabla w_j \, dV = |\Omega_k| \nabla w_i \cdot \nabla w_j$$

which depend only on the FE mesh and not on γ. These coeficients can be pre-calculated during the mesh generation saving considerable time in the system assembly. An alternative is to define a discrete gradient operator $D : \mathbb{C}^N \to \mathbb{C}^{3K}$ which takes the representation as a vector of vertex values of a piecewise linear function ϕ to the vector of $\nabla\phi$ on each simplex (on which of course the gradient is constant). On each simplex define $\Sigma_k = (\gamma_k/|\Omega_k|)\mathbf{I}_3$ where $\mathbf{I}_3$ is the 3×3 identity matrix, or for the anisotropic case simply the conductivity matrix on that simplex divided by its volume, and $\Sigma = \operatorname{diag}(\Sigma_k) \otimes \mathbf{I}_K$. We can now use

$$A_M = D^T \Sigma D \tag{1.58}$$

to assemble the main block of the system matrix.

Box 1.5: FEM as a resistor network

It may help to think of the finite element method in terms of resistor networks. For the case we have chosen with piecewise linear potentials on simplicial cells and conductivity constant on cells there is an exact equivalence [129]. To construct a resistor network equivalent to such a FEM model replace each edge by a resistor. To determine the conductance of that resistor consider first a triangle (in the two dimensional case), and number the angles θ_j opposite the j-th side. The resistor on side j has a conductance $\sigma\cot\theta_i$. When the triangles are assembled in to a mesh the conductances add in parallel summing the contribution from triangles both sides of an edge. In the three dimensional case θ_j is the angle between the two faces meeting at the edge opposite edge j, and of course several tetrahedra can meet at one edge.

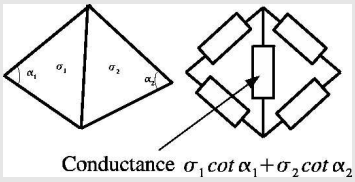

The corresponding resistor network for a 2D FEM mesh

With a resistor mesh assembled in this way, voltages ϕ_i at vertex i are governed by Ohms law and Kirchoff's law, and the resulting system of equations is identical to that derived from the FEM. The situation is not reversible as not all resistor networks are the graphs of edges of two or three dimensional a FE mesh. Also some allocation of resistances do not correspond to a piecewise constant isotropic conductivity. For example there may be no consistent allocation of angles θ_j so that around any given vertex (or edge in 3D) they sum to 2π.
The question of uniqueness of solution, as well as the structure of the transconductance matrix for real planar resistor networks well understood [**?**, 40].

1.8.2 Solving the linear system

We now consider the solution of the system (1.52). The system has the following special features. The matrix is sparse, the number of non-zeros in each row of the main block depends on the number of neighbouring verticies connected to any given vertex by an edge. It is symmetric(for complex conductivity and contact impedance that means real and imaginary parts are symmetric), and the real part is positive definite. In addition, we have multiple righthand sides for the same conductivity, and we wish to solve the system repeatedly for similar

conductivities.

A simple approach to solving $\mathbf{Ax} = \mathbf{b}$ is LU-factorization [61], where an upper triangular matrix $\mathbf{U}$ and lower triangular matrix $\mathbf{L}$ are found such that $\mathbf{A} = \mathbf{LU}$. As solving a system with a diagonal matrix is trivial, one can solve $\mathbf{Lu} = \mathbf{b}$ (forward substitution) and then $\mathbf{Ux} = \mathbf{u}$ (backward substitution). The factorization process is essentially Gaussian elimination and has a computational cost $O(n^3)$ while the backward and forward substitute have a cost $O(n^2k)$ for k righthand sides.. An advantage of a factorization method such as this is that one can apply the factorization to multiple right hand sides, in our case for each current pattern. Although the system matrix is sparse, the factors are in general less so. Each time a row is used to eliminate the non-zero elements below the diagonal it can create more non-zeros above the diagonal. As a general rule it is better to reorder the variables so that rows with more non-zeros are further down the matrix. This reduces the *fill in* of non-zeros in the factors. For a real symmetric or Hermittian matrix the Symmetric Multiple Minimum Degree Algorithm [50] reduces fill in, whereas the Column Multiple Minimum Degree algorithm is designed for the general case. For an example see Figure 1.4. The renumbering should be calculated when the mesh is generated so that it is done only once.

For large 3D systems direct methods can be expensive and iterative methods may prove more efficient. A typical iterative scheme has a cost of $O(n^2k)$ per iteration and requires fewer than n iterations to converge. In fact the number of iterations required needs to be less than Cn/k for some C depending on the algorithm to win over direct methods. Often the number of current patterns driven is limited by hardware to be small while the number of verticies in a 3D mesh needs to be very large to accurately model the electric fields, and consequently iterative methods are often preferred in practical 3D systems. The potential for each current pattern can be used as a starting value for each iteration. As the adjustments in the conductivity become smaller this reduces the number of iterations required for forward solution. Finally it is not necessary to predict the voltages to full floating point accuracy when the measurements system itself is far less accurate than this, again reducing the number of iterations required.

The convergence of iterative algorithms, such as conjugate gradient method (see Sec 1.8.3, can be improved by replacing the original system by $\mathbf{PAx} = \mathbf{Pb}$ for some matrix $\mathbf{P}$ which is an approximation to the inverse of $\mathbf{A}$. A favourite choice is to use an approximate LU- factorization. In EIT one can use the same preconditioner over a range of conductivity values.

1.8.3 Conjugate Gradient and Krylov subspace methods

The conjugate gradient (CG) method [17, 61] is a fast and efficient method for solving $\mathbf{Ax} = \mathbf{b}$ for real symmetric matrices $\mathbf{A}$ (as well as Hermitian complex matrices) . The method generates a sequence $\mathbf{x}_i$ (iterates) of successive approximations to the solution and residuals $\mathbf{r}_i = \mathbf{b} - \mathbf{Ax}_i$ and search directions $\mathbf{p}_i$ and $\mathbf{q}_i = \mathbf{Ap}_i$ used to update the iterates and residuals. The update to the

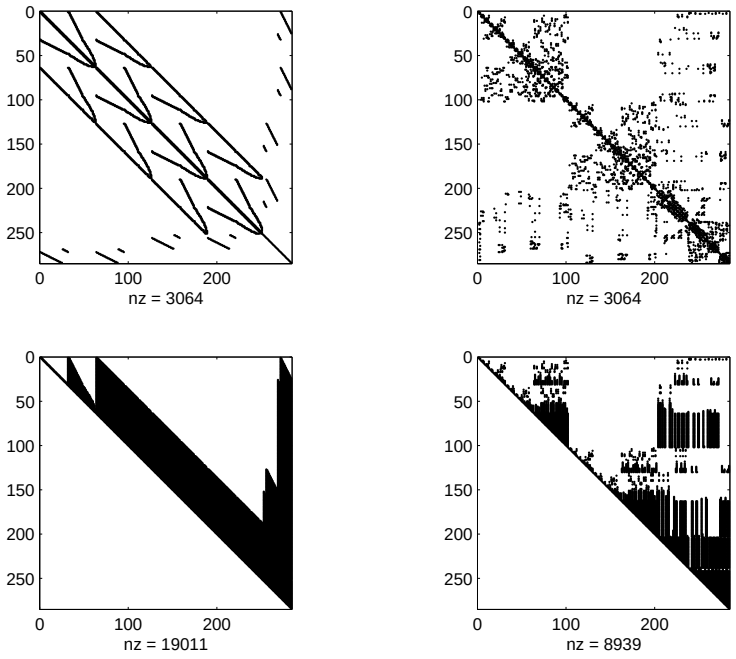

Figure 1.4: Top left the sparsity pattern of a system matrix which is badly ordered for fillin. Bottom left sparsity pattern for the U factor. On the right the same after reordering with `colmmd`.

iterate is

$$\mathbf{x}_i = \mathbf{x}_{i-1} + \alpha_i \mathbf{p}_i \tag{1.59}$$

where the scalar α_i is chosen to minimize

$$\mathbf{r}(\alpha)^* \mathbf{A}^{-1} \mathbf{r}(\alpha) \tag{1.60}$$

where $\mathbf{r}(\alpha) = \mathbf{r}_{i-1} - \alpha \mathbf{r}_{i-1}$ explicitly

$$\alpha_i = \frac{\|\mathbf{r}_{i-1}\|^2}{\mathbf{p}_i^* \mathbf{A} \mathbf{p}_i}. \tag{1.61}$$

The search directions are updated by

$$\mathbf{p}_i = \mathbf{r}_i + \beta_{i-1} \mathbf{p}_{i-1} \tag{1.62}$$

where using

$$\beta_i = \frac{\|\mathbf{r}_i\|^2}{\|\mathbf{r}_{i-1}\|^2} \tag{1.63}$$

ensures that $\mathbf{p}_i$ are orthogonal to all $\mathbf{A}\mathbf{p}_j$ and $\mathbf{r}_I$ are orthogonal to all $\mathbf{r}_j$, for $j < i$. The iteration can be terminated when the norm of the residual falls below a predetermined level.

Conjugate Gradient Least Squares (CGLS) method solves the least squares problem (1.7) $\mathbf{A}^T\mathbf{A}\mathbf{x} = \mathbf{A}^T\mathbf{b}$ without forming the product $\mathbf{A}^T\mathbf{A}$ (also called CGNR or CGNE Conjugate Gradient Normal Equations [29, 17]) and is a particular case of the non-linear conjugate gradient (NCG) algorithm of Fletcher and Reeves [47](see also [151, Ch 3]). The NCG method seeks a minimum of a cost functions $f(\mathbf{x}) = \frac{1}{2}\|\mathbf{b} - F(\mathbf{x})\|^2$, which in the case of CGLS is simply the quadratic $\frac{1}{2}\|\mathbf{b} - \mathbf{A}\mathbf{x}\|^2$. The direction for the update in (1.59) is now

$$\mathbf{p}_i = -\nabla f(\mathbf{x}_i) = \mathbf{J}_i^*(\mathbf{b} - F(\mathbf{x}_i)) \tag{1.64}$$

where $\mathbf{J}_i = F'(\mathbf{x}_i)$ is the Jacobian. How far along this direction to go is determined by

$$\alpha_i = \arg\min_{\alpha>0} f(\mathbf{x}_{i-1} + \alpha \mathbf{p}_i) \tag{1.65}$$

which for non-quadratic f requires a line search.

CG can be used for solving the EIT forward problem for real conductivity, and has the advantage that it is easily implemented on parallel processors. Faster convergence can be used using a preconditioner, such as an incomplete Cholesky factorization,chosen to work well with some predefined range of conductivities. For the non Hermitian complex EIT forward problem, and the linear step in the inverse problem,other methods are needed. The property of orthogonal residuals for some inner product (Kylov subspace property) of CG is shared by a range of iterative methods. Relatives of CG for non-symmetric matrices include Generalised Minimal Residual (GMRES) [121], Bi-Conjugate Gradient BiCG, Quasi Minimal Residual (QMR) and Bi-Conjugate Gradient Stabilized (Bi-CGSTAB). All have their own merits [17] and as implementations are readily available have been tried to some extent in EIT forward or

inverse solutions, not much [91, 63] is published but applications of CG itself to EIT include [114, 117, 102, 109] and to optical tomography [5, 6]. The application Krylov subspace methods to solving elliptic PDEs as well as linear inverse problems [65, 29] are active areas of research and we invite the reader to seek out and use the latest developments.

1.8.4 Mesh generation

Mesh generation is a major research area in itself, and posses particular challenges in medical EIT. The mesh must be fine enough to represent the potential with sufficient accuracy to predict the measured voltages as a function of conductivity. In medical EIT this means we must adequately represent the surface shape of the region to be images, and the geometry of the electrodes. The mesh needs to be finer in areas of high field strength and this means in particular near the edges of electrodes. Typically there will be no gain in accuracy from using a mesh in the interior which is as fine. As we are usually not interested so much in conductivity changes near the electrodes, and in any case we cannot hope to resolve conductivity on a scale smaller than the electrodes, our parameterization of the conductivity will inevitably be coarser than the potential. One easy option is to choose groups of tetrahedra as voxels for conductivity, another is to use basis functions interpolated down to the FE mesh. If there are regions of known conductivity, or regions where the conductivity is known to be constant, the mesh should respect these regions. Clearly the electric field strengths will vary with the current pattern used, and it is common practice to use a mesh which is suitable for all current patters, which can mean that it would be unnecessarily fine away from excited electrodes. The trade-off is that the same system matrix is used for each current pattern.

Any mesh generator needs to have a data structure to represent the geometry of the region to be meshed. This includes the external boundary shape, the area where the electrodes are in contact with the surface and any internal structures. Surfaces are can represented either as a triangularization, or more by more general polygons, or by spline patches. The relationship between named volumes, surfaces curves and points must also be maintained usually as a tree or incidence matrix. Simple geometric objects can be constructed from basic primitive shapes, either with a graphical user interface or from a series of commands in a scripting language. Set theoretic operations such as union, intersection can be performed together with geometric operations such as extrusion (for example of a circle into a cylinder).

As each object is added consistency checks are performed and incidence data structures maintained. For general objects these operations require difficult and time consuming computational geometry.

For examples of representations of geometry and scripting languages see the documentation for QMG [149], Netgen [125] and FEMLAB [33].

Commercial Finite Element software can often import geometric models from Computer Aided Design programs, which makes life easier for industrial applications. Unfortunately human bodies are not supplied with blueprints from their

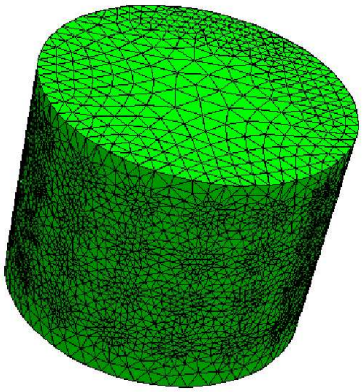

Figure 1.5: A mesh generated by NETGEN for a cylindrical tank with circular electrodes

designer. The problem of creating good FE meshes of the human body remains a significant barrier to progress in EIT, and of course such progress would also benefit other areas of biomedical electromagnetic research. One approach [12] is to segment Nuclear Magnetic Resonance, or X-Ray CT images and use these to develop a FE mesh specific to an individual subject. Another is to warp a general anatomical mesh to fit the external shape of the subject [54], measured by some simpler optical or mechanical device.

Once the geometry is defined, one needs to create a mesh. Mesh generation software generally use a combination of techniques such as advancing front, octtree [150], bubble-meshing [128]. In a convex region given a collection of verticies, a tetrhedral mesh of their convex hull can be found with the Delaunay property that no tetrahedron contains any vertex in the interior of its circumsphere, using the QuickHull algorithm [7].

The standard convergence results for the FEM, [137] require that as the size of the tetrahedra tend to zero the ratio of the circumscribing sphere to inscribing sphere is bounded away from zero. In practice this means that for an isotropic medium without *a priori* knowledge of the field strengths tetrahedra which are close to equilateral are good and those with a high aspect ratio are bad. Mesh generator typically include methods to *smooth* the mesh. This simplest is *jiggling* in which each interior vertex in turn is moved to the center of mass of the polyhedron defined by the verticies with which it shares an edge (its neighbours). This can be repeated for some fixed number of iterations or until the shape of the elements ceases to improve. Jiggling can be combined with removal of edges

and swapping faces which divide polyhedra into two tetrahedra. In EIT where the edges of electrodes and internal surfaces need to be preserved this process is more involved.

1.9 Measurement Strategy

In EIT we seek to measure some discrete version of Λ_γ or Λ_γ^{-1}. We can choose the geometry of the system of electrodes, the excitation pattern and the measurements that are made. We have to strike a balance between the competing requirements of accuracy, speed and simplicity of hardware.

Once a system of electrodes of L has been specified the complete relationship between current and voltage at the given frequency is summarized by the transfer impedance matrix $\mathbf{Z} \in \mathbb{C}^{L\times L}$. The null space of $\mathbf{Z}$ is spanned by the constant vector $\mathbf{1}$, and for simplicity we set the sum of voltages also to be zero $\mathbf{1Z} = 0$ so that $\mathbf{Z}$ is symmetric $\mathbf{Z} = \mathbf{Z}^T$ (note transpose not conjugate).

1.9.1 Linear Regression

We will illustrate the ideas mainly using the assumption that currents are prescribed and the voltages measured, although there are systems which do the opposite. In this approach we regard the matrix of voltage measurements to be contaminated by noise, while the currents are known accurately. This should be compared with the familiar problem of linear regression where we aim to fit a straight to experimental observations. Assuming a relation of the form $y = ax$. For will assume an intercept of zero and mean $\overline{x}$ of zero. The abscissae x_i are assumed accurate and the y_i contaminated with noise. Assembling the x_i and y_i into *row* vectors $\mathbf{x}$ and $\mathbf{y}$ we estimate the slope a by

$$\hat{a} = \arg\,\min_a \|\mathbf{y} - a\mathbf{x}\|^2. \tag{1.66}$$

Of course the solution is $a = \mathbf{y}\mathbf{x}^\dagger$, another way of expressing the usual regression formulae. The least squares approach can be justified statistically [106] Assuming the errors in $\mathbf{y}$ have zero correlation $\hat{a}$ is an unbiased estimator for a. Under the stronger assumption that the y_i are independently normally distributed with identical variance $\hat{a}$ is the maximum likelihood estimate of a, and is normally distributed with mean a. Under these assumptions we can derive confidence intervals and hypothesis testing for a [106, p14].

Although less well known, linear regression for several independent variables follows a similar pattern. Now X and Y are matrices and we seek a linear relation of the form $Y = AX$. The estimate $\hat{A} = YX^\dagger$ has the same desirable statistical properties as the single variable case [106, Ch 2].

Given a system of K current patterns assembled in a matrix $I \in \mathbb{C}^{L\times K}$ (with column sums zero) we measure the corresponding voltages are $V = \mathbf{Z}I$. Assuming the currents are accurate but the voltages contain error we then obtain our estimate $\hat{\mathbf{Z}} = VI^\dagger$. If we have two few linearly independent currents

rank $I < L-1$ then this will be an estimate of a projection of $\mathbf{Z}$ on to a subspace, if we have more than $L-1$ current patterns then the generalized inverse averages over the redundancy, reducing the variance of $\hat{\mathbf{Z}}$. Similarly we can make redundant measurements. let $\mathbf{M} \in \mathbb{R}^{M \times L}$ be a matrix containing the measurement patterns used (for simplicity the same for each current pattern), so that we measure $V_M = MV$. Our estimate for $\mathbf{Z}$ is now $M^\dagger V_M I^\dagger$. Again redundant measurements will reduce variance. Of course it is common practice to take multiple measurements of each voltage (X-REF), and the averaging of these may be performed within the data acquisition system before it reaches the reconstruction program. In this case the effect is identical to using the generalized inverse. The benefit in using the generalized inverse is that it automatically averages over redundancy where there are multiple linearly dependent measurements. If quantization in the Analogue to Digital Converter (ADC) is the dominant source of error, averaging over different measurements reduces the error, in a similar fashion to *dithering* (adding a random signal and averaging) to improve the accuracy of an ADC. Some EIT systems use variable gain amplifiers before voltage measurements are passed to the ADC. In this case the absolute precision varies between measurements and a weighting must be introduced in the norms used to define the least squares problem.

For the case where the voltage is accurately controlled and the current measured an exactly similar argument holds for estimating the transfer admittance matrix. However where there are errors in both current and voltage, for example caused by imperfect current sources, a different estimation procedure is required. What we need is *multiple correlation analysis* [106, p82] rather than multiple regression.

One widely used class of EIT systems which use voltage drive and current measurement are ECT systems used in industrial process monitoring [27]. Here each electrode is excited in turn with a positive voltage while the others are at ground potential. The current flowing to ground through the non-driven electrode is measured. Once the voltages are adjusted to have zero mean this is equivalent to using the basis (1.57) for $\mathbf{Y}|_S$.

We know that feasible transfer impedance matrices are symmetric and so employ the orthogonal projection on to the feasible set and replace $\hat{\mathbf{Z}}$ by $\operatorname{sym} \hat{\mathbf{Z}}$ where $\operatorname{sym} A = \frac{1}{2}(A + A^T)$. This is called *averaging over reciprocity error*. The skew-symmetric component of the estimated $\mathbf{Z}$ gives an indication of errors in the EIT instrumentation. (X-REF)

1.9.2 Sheffield Measurement Protocol

The space of contact impedances is a subset of the vector space of symmetric $L \times L$ matrices with column and row sums zero, which has dimension $L(L-1)/2$. In addition the real part of $\mathbf{Z}|_S$ is positive definite, otherwise there would be direct current patterns which dissipate no power. There are other conditions on $\mathbf{Z}$, given in the plane case by [**?**], associated with Ω being connected, and its is shown in the planar case that the the set of feasible $\mathbf{Z}$ is an open subset of the vector space descried above. This confirms that we can measure up to

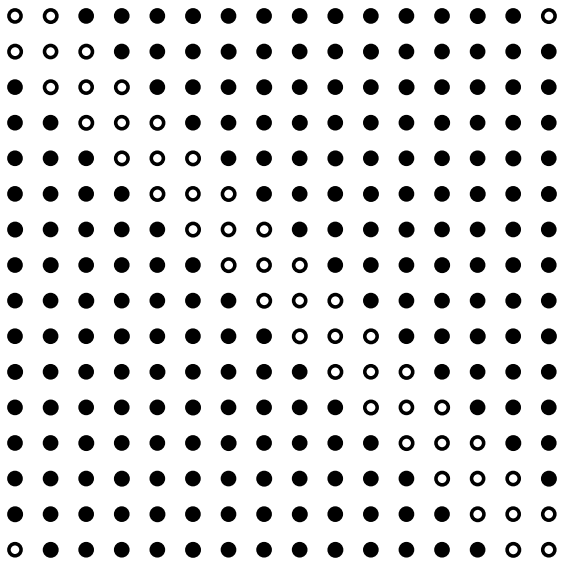

Figure 1.6: Each column corresponds to a drive pair and each row to a measurement pair. A • indicates a measurement that s taken and a ∘ one which is not omitted.

$L(L-1)/2$ independent parameters. Some systems however measure fewer than this, primarily to avoid measuring voltage on actively driven electrodes.

The Sheffield Mark I and II systems [11] use a protocol with $L = 16$ electrodes which are typically arranged in a circular pattern on the subject. Adjacent pairs E_l, E_{l+1} are excited with equal and opposite currents, for L ranging from 1 to $L-1$. These can be assembled in to a matrix $I_{\mathrm{P}} \in \mathbb{R}^{L\times(L-1)}$ with $\delta_{lk} - \delta_{l\,k+1}$ in the $l\,k$ position. Clearly the columns of I_{P} span S. Measurements are made similarly between adjacent pairs and I_{P}^T gives the measurement patterns so that the matrix of all possible voltages measured is $\mathbf{Z}_{\mathrm{P}} = I_{\mathrm{P}}^T Z I_{\mathrm{P}}$, a symmetric $(L-1)\times(L-1)$ matrix of full rank. However when the l-th electrode pair is excited, the measurement pairs $l-1, l$ and $l+1$ are omitted (indices are assumed to wrap around when out of range). The subset of $\mathbf{Z}_{\mathrm{P}}$ which is actually measured by the Sheffield system is shown in Figure 1.6 and a simple counting argument shows that the number of independent measurements is $(L-2)(L-1)/2 - 1 = L(L-3)/2$, or 104 for $L = 16$.

In practice a Sheffield mark I or II system aiming at speed rather than accuracy measures a non redundant set of exactly 104 measurement. For the first two drive patterns all 15 pairs are measured, and for subsequent drives one less is measured each time. If reciprocity error is very small this is an acceptable strategy.

A pair drive system has the advantage that only one current source is needed, which can then be switched to each electrode pair. With a more complex switch-

ing network other pairs can be driven at the expense of higher system cost and possibly a loss of accuracy. A study of the dependence of the SVD of the Jacobian for different separations between driven electrodes can be found in [23]

One feature of the Sheffield protocol is that on a two dimensional domain the adjacent voltage measurements are all positive. This follows as the potential itself is monotonically decreasing from source to sink. The measurements also have a 'U' shaped graph for each drive. This provides an additional feasibility check on the measurements. Indeed if another protocol is used Sheffield data $\mathbf{Z}_{\mathrm{P}}$ can be synthesized to employ this check.

1.9.3 Optimal Drive Patterns

The problem of optimizing the drive patterns in EIT was first considered by Seagar [126] who calculated the optimal placing of a pair of point drive electrodes on a disk to maximize the voltage differences between the measurement of a homogeneous background and an offset circular anomaly. Isaacson [73], and Gisser, Isaacson and Newell [55] argued that one should choose a single current pattern to maximize the L^2 norm of the voltage difference between the measured $\mathbf{V}_m$ and calculated $\mathbf{V}_c$ voltages constraining the L^2 norm of the current patterns in a multiple drive system. This is a simple quadratic optimization problem

$$I_{\mathrm{opt}} = \arg\,\min_{I\in S} \frac{\|(\mathbf{V}_m - \mathbf{V}_c)I\|}{\|I\|} \tag{1.67}$$

to which the answer is that I_{opt} is the eigenvector of $|\mathbf{Z}_m - \mathbf{Z}_c|$ corresponding to the largest eigenvalue (here $|\mathbf{A}| = (\mathbf{A}^*\mathbf{A})^{1/2}$ One can understand this eigenvector to be a current pattern which focuses the dissipated power in the regions where actual and predicted conductivity differs most. If one is to apply only one current pattern then in a particular sense this is best. The eigenvectors for smaller eigenvalues are increasingly less useful for telling these two conductivities apart and one could argue that eigenvectors for eigenvalues which are smaller than the error in measurement contain no useful information. In [55] it is argued that the eigenvector for this eigenvalue can be found experimentally using the *power method* a classical fixed point algorithm for numerically finding an eigenvector.

Later [56] used a constraint on the maximum dissipated power in the test object which results in the quadratic optimization problem

$$I_{\mathrm{opt}} = \arg\,\min_{I\in S} \frac{\|(\mathbf{V}_m - \mathbf{V}_c)I\|}{\|\mathbf{V}_m^* I\|} \tag{1.68}$$

which is a generalized eigenvalue problem. The argument here is that the dissipated (and stored) power should be limited in a medical application, rather than the rather artificial constraint of sum of squares of current.

Optimal current patterns can be incorporated in iterative reconstruction algorithms, at each iteration the optimal currant pattern to distinguish between the actual and conductivity and the latest approximation can be applied, and

the voltage data from this pattern used in the next iterative update. As the current pattern used will change at each iteration eventually all the information in $\mathbf{Z}_m$ will be used. Alternatively more than one of the eigenvectors of $|\mathbf{Z}_m - \mathbf{Z}_c|$ can be used, provided the resulting voltages differences are above the noise level. In practice this method is an improvement over pair drives even for simulated data [25].

Driving current patterns in eigenvectors requires multiple programmable current sources with consequent increase in cost and complexity. There is also the possibility that a pair drive system could be made with sufficiently better accuracy that it counteracts the advantage of a multiple drive system with optimal patterns. Even neglecting the errors in measurement, there is numerical evidence [24] that using optimal currents produces better reconstructions on synthetic data. In this respect one can also use synthetic optimal voltage patterns [111].

The framework used to define optimal current patterns is the ability to distinguish between two transfer impedance matrices. In the context of reconstruction algorithms, we can use an inability to distinguish between $\mathbf{Z}_c$ and $\mathbf{Z}_m$ to measurement accuracy as a stopping criterion for an iterative algorithm. In another context we can consider hypothesis testing, in the classical statistical sense. As an example suppose we have reconstructed an EIT image of a breast that shows a small anomaly in a homogeneous background – perhaps a tumour. We can test the hypothesis that $\mathbf{V}_m - \mathbf{V}_c$ and $\mathbf{I}$ are not linearly related, that is the null hypothesis $H_0 : \mathbf{Z}_m - \mathbf{Z}_c = 0$. Which can be tested using a suitable statistic with an F-distribution [106, p133]. If only one current normalized pattern is used the optimal current will give a test with the greatest *power*. In the statistical terminology power is the conditional probability that we reject the hypothesis H_0 given that it is false.

Eyöboğlu and Pilkington [46] argued that medical safety legislation demanded that one restrict the maximum total current entering the body, and if this constraint was used the distinguishability is maximized by pair drives. Cheney and Isaacson [35] study a concentric anomaly in a disk, using the 'gap' model for electrodes. They compare trigonometric, Walsh, and opposite and adjacent pair drives for this case giving the dissipated power as well as the L^2 and power distinguishabilies. Köksal and Eyöboğlu [79] investigate the concentric and offset anomaly in a disk using continuum currents. Further study of optimization of current patterns with respect to constraints can be found in [87]

1.10 Numerical Examples

In this section we exhibit some numerical examples to illustrate points made elsewhere in the text. The forward simulations are done on modest meshes, so that readers may repeat the experiments themselves without excessive computational requirements. It is not our intention to present these results as the state of the art, although we do intend to indicate that the use of a 3D forward model, and CEM boundary conditions should be a minimal starting point for

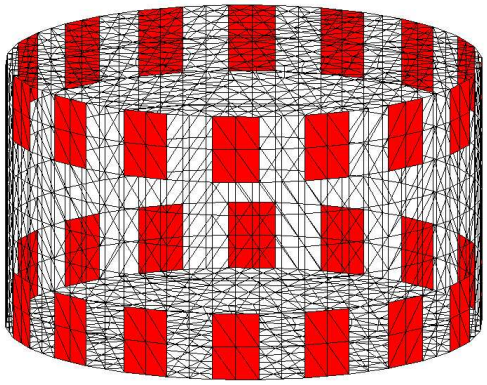

Figure 1.7: Mesh used for potentials in reconstruction A courser meshof which this is a subdivision, was used to represent the conductivity

testing EIT reconstruction algorithms, so that they have a chance of fitting experimental data. In addition to the smoothly regularized Gauss-Newton method of Sec 1.5.3 we also exhibit PD-IPM for solution of the TV regularized problem of Sec 1.6. To our knowledge the first such results for 3D EIT.

The simulated data, using a finer mesh than that used for reconstruction, models a cylinder with 28 rectangular electrodes on the curved side (Figure 1.7). First we reconstruct a smooth conductivity of the form $\sigma(x, y, z) = 3 + x + y + z + 10z$ (Figure 1.8). Of course using a smoothing prior this is relatively easy to recover. The reconstruction, using a courser mesh, is the standard regularized Gauss-Newton using an approximation to the Laplacian for $\mathbf{L}$, very similar to the examples in the EIDORS 3D code [115]. The results of the reconstruction are shown in Figure 1.8. The reconstruction was also performed with TV regularization using the PD-IPM code of Borsic [13]. The results (Figure **??**) exhibit the characteristic "blocky" image which reflects the prior distribution inherent in TV regularization.

By contrast, a test object consisting of two homogeneous spheres of higher conductivity (Figure 1.9) was reconstructed with both smooth and TV regularization, Figure 1.10. The TV regularization is clearly superior at recovering the jump change in conductivity.

The reconstructions in this section were performed with synthetic data with Gaussian pseudo-random noise. The reconstructions degraded significantly when the standard deviation of the noise went above ??.

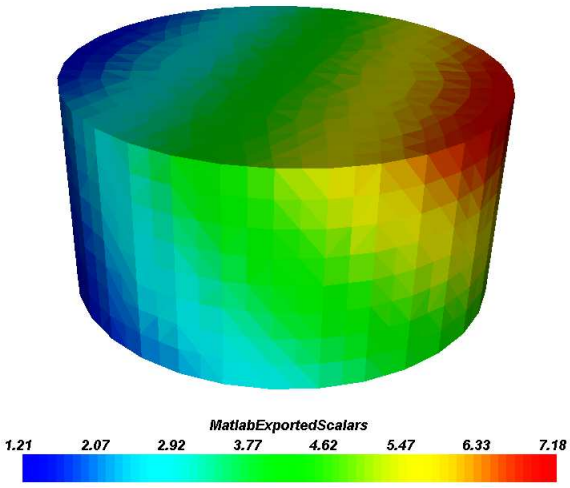

(a) Original smooth conductivity distribution projected on to the courser mesh (Mayavi surface map)

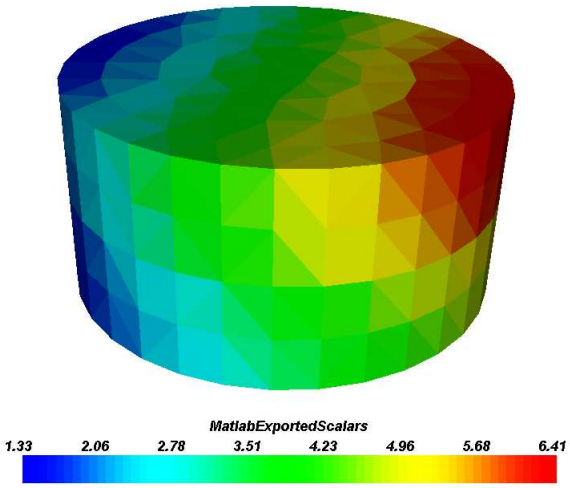

(b) Smoothly regularized Gauss-Newton reconstruction of this smooth conductivity

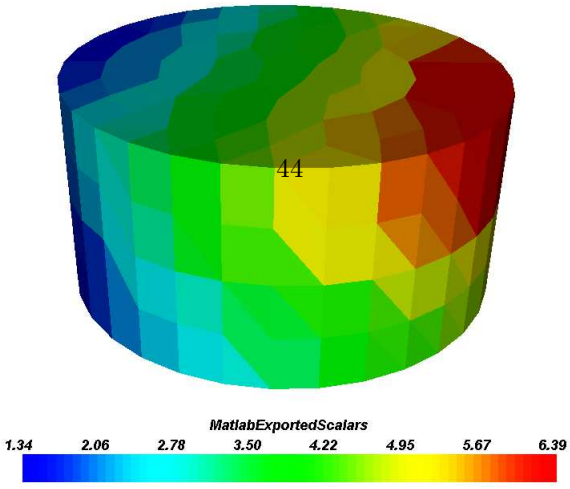

(c) TV regularized PD-IPM reconstruction of the same smooth

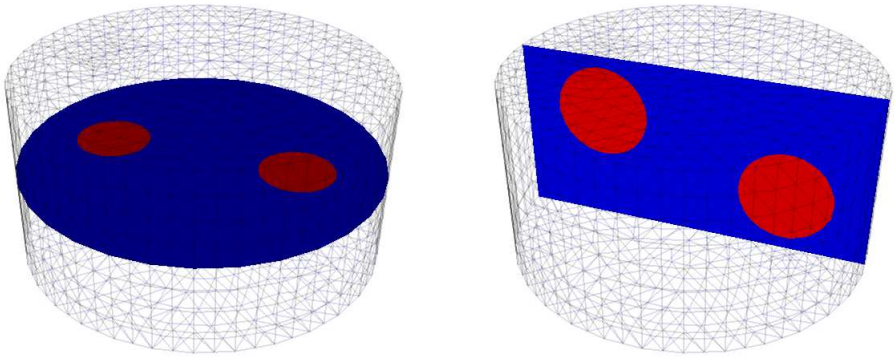

(a) The test object consisted of two spheres of conductivity 1 in a background of 3. An unrelated finer mesh was used to generate the simulated data

Figure 1.9: Electrodes, mesh and two spheres test object

1.11 Common Pitfalls and Best Practice

The ill-posed nature of inverse problems means that any reconstruction algorithm will have limitations on what images it can accurately reconstruct and that the images degrade with noise in the data. When developing a reconstruction algorithm it is usual to test it initially on simulated data. Moreover the reconstruction algorithms typically incorporates a forward solver. A natural first test is to use the same forward solver to generate simulated data with no simulated noise and to then find to one's delight that the simulated conductivity can be recovered fairly well, the only difficulties being if it violates the *a priori* assumptions built into the reconstruction and the limitations of floating point arithmetic. Failure of this basic test is used as a diagnostic procedure for the program. On the other hand, claiming victory for ones reconstruction algorithm using this data is what is slightly jokingly called an 'inverse crime" [41, p133] (by analogy with the "variational crimes" in FEM perhaps). We list a few guidelines to avoid be accused of an inverse crime and to lay out what we believe to be best practice. For slightly more details see [88].

1. **Use a different mesh.** If you do not have access to a data collection system and phantom tank, or if your reconstruction code is at an early stage of development, you will want to test with simulated data. To simulate the data use a finer mesh than is used in the forward solution part of the reconstruction algorithm. But not a strict refinement. You shape of any conductivity anomalies in the simulated data should not

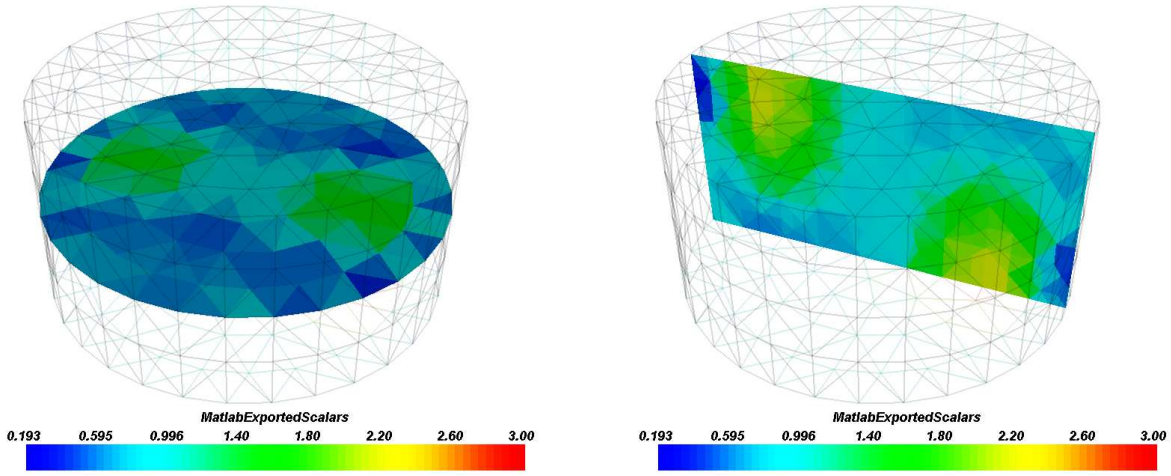

(a) Regularized Gauss-Newton reconstruction, shown using cut-planes

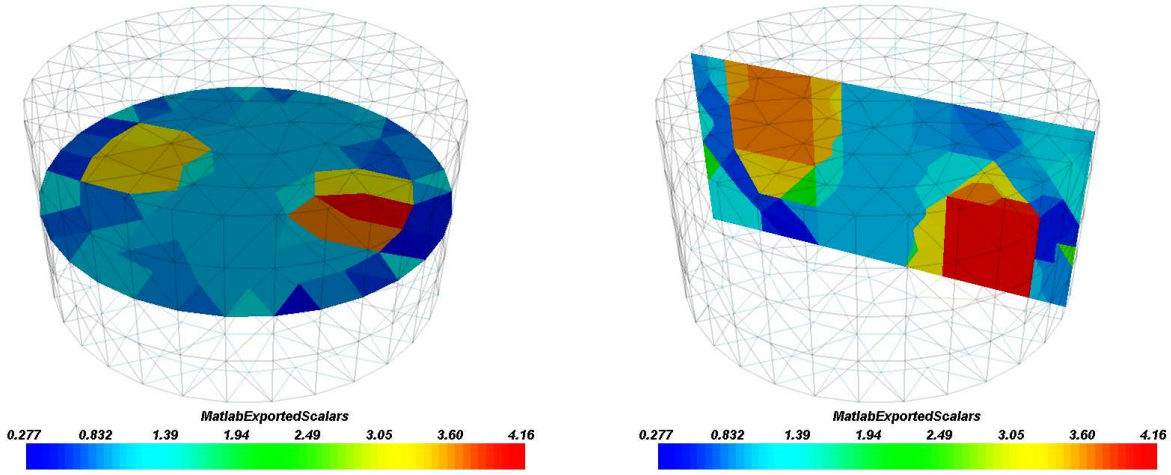

(b) Total Variation reconstruction from PD-IPM

Figure 1.10: Reconstruction of a two spheres test object from Figure 1.9 using Regularized Gauss-Newton and TV PD-IPM.

exactly conform with the reconstruction mesh, unless you can assume the shape is known *a priori*.

2. **Simulating noise.** If you are simulating data you must also simulate the errors in experimental measurement. At the very least there is quantisation error in the analogue to digital converter. Other sources of error include stray capacitance, gain errors, inaccurate electrode position, inaccurately known boundary shape, and contact impedance errors. To simulate errors sensibly it is necessary to understand the basics of the data collection system, especially when the gain on each measurement channel before the ADC is variable. When the distribution of the voltage measurement errors is decided this is usually simulated with a pseudo random number generator.

3. **Pseudo random numbers.** A random number generator models a draw from a population with a given probability density function. To test the robustness of your reconstruction algorithm with respect to the magnitude of the errors it is necessary to make repeated draws, or calls to the random number generator, and to study the distribution of reconstruction errors. As our inverse problem is non-linear even a Gaussian distribution of error will not produce a (multivariate) Gaussian distribution of reconstruction errors. Even if the errors are small and the linear approximation good, at least the mean and variance should be considered.

4. **Not tweaking.** Reconstruction programs have a number of adjustable parameters such as Tikhonov factors and stopping criteria for iteration, as well as levels of smoothing, basis constraints and small variations of an algorithms. While there are rational ways of choosing reconstruction parameters based on the data (such as generalized cross validation and L-curve), and on an estimate of the data error (Morotzov's stopping criterion). In practice on often finds acceptable values empirically which work for a collection of conductivities one expects to encounter.There will always be other cases for which those parameter choices do not work well. What one should avoid is *tweaking* the reconstruction parameters for each set of data until one obtains an image which one knows is close to the real one. By contrast an honest policy is to show examples of where a certain algorithm and parameters performs poorly as well as the best examples.

1.12 Further Developments in Reconstruction Algorithms

In this review there is not space to describe in any detail many of the exciting current development in reconstruction algorithms. Before highlighting some of these developments it is worth emphasizing that for illposed problem *a priori* information is essential for a stable reconstruction algorithms, and it is better that this information is incorporated in the algorithm in a systematic and

transparent way. Another general principle of inverse problems is to think carefully what information is required by the end user. Rather than attempting to produce an accurate image what is often required in medical (and indeed most other) applications is an estimate of a much smaller number of parameters which can be used for diagnosis. For example we may know that a patient has two lungs as well as other anatomical features but we might want to estimate their water content to diagnose pulminary oedema. A sensible strategy would be devise an anatomical model of the thorax and fit a few parameters of shape and conductivity rather than pixel conductivity values. The disadvantage of this approach is that each application of EIT gives rise to its own specialised reconstruction method, which must be carefully designed for the purpose. In the author's opinion the future development of EIT systems, including electrode arrays and data acquisition systems as well as reconstruction software, should focus increasingly on specific applications, although of course such systems will share many common components.

1.12.1 Beyond Tikhonov regularization

We have also discussed the use of more general regularization functionals including total variation. For smooth G traditional smooth optimization techniques can be used, whereas for Total Variation the PD-IPM is promising. Other functionals can be used to penalize deviation from the *a priori* information, one such choice is the addition of the Mumford-Shah functional which penalizes the Hausdorf measure of the set of discontinuities [119]. In general there is a trade-off between incorporating accurate *a priori* information and speed of reconstruction. Where the regularization matrix $\mathbf{L}$ is discretized partial differential operator, the solution of the linearized problem is a compact perturbation of a partial differential equation. This suggests that multigrid methods may be used in the solution of the inverse problem as well. For a single linearized step this has been done for the EIT problem by McCormick and Wade [101], and for the non-linear problem by Borcea [18]. In the same vein adaptive meshing can be used for the inverse problem as well as the forward problem [102, 103, 92]. In both cases there is the interesting possibility to explore the interaction between the meshes used for forward and inverse solution.

At the extreme end of this spectrum we would like to describe the prior probability distribution and for a known distribution of measurement noise and calculate the entire posterior distribution. Rather than giving one image, such as the MAP estimate gives a complete description of the probability of any image. If the probability is bimodal for example, one could present the two local maximum probability images. If one needed a diagnosis, say of a tumour, the posterior probability distribution could be used to calculate the probability that a tumour like feature was there. The computational complexity of calculating the posterior distribution for all but the simplest distributions is enormous, however the posterior distribution can be explored using the Markov Chain Monte Carlo Method (MCMC) which has been applied to two dimensional EIT [76]. This was applied to simulated EIT data [49], and more recently to tank data,

for example [105] For this to be a viable technique for the 3D problem highly efficient forward solution will be required.

1.12.2 Direct non-linear methods

Iterative methods which use optimization methods to solve a regularized problem are necessarily time consuming. The forward problem must be solved repeatedly and the calculation of an updated conductivity is also expensive. The first direct method to be proposed was the Layer Stripping algorithm [130] however this is yet to be shown to work well on noisy data. An exciting recent development is the implementation of a Scattering Transform ($\overline{\partial}$ or d-bar) algorithm proposed by Nachman. Siltanen *et al* [127] showed that this can be implemented stably and applied to *in vitro* data [99]. The main limitation of this technique is that is inherently two dimensional and no one has found a way to extend it to three dimensions, also in contrast to the more explicit forms of regularization it is not clear what *a priori* information is incorporated in this method as the smoothing is applied by filtering the data. A strength of the method is its ability to accurately predict absolute conductivity levels. In some cases where long electrodes can be used and the conductivity varies slowly in the direction in which the electrodes are oriented a two dimensional reconstruction may be a useful approximation. This is perhaps more so in industrial problems such as monitoring flow in pipes with ECT or ERT. In some situations a direct solution for a two dimensional approximation could be used as a starting point for an iterative three dimensional algorithm.

Two further direct methods show considerable promise for specific applications. The monotonicity method of Tamburrino and Rubinacci [139] relies on the monotonicity of the map $\rho \mapsto R_\rho$ where ρ is the real resistivity and R_ρ the transfer resistance matrix. This method, which is extremely fast, relies on the resistivity of the body to be known to be one of two values. It works equally well in two and three dimensions and is robust in the presence of noise. The time complexity scales linearly with the number of voxels (which can be any shape) and scales cubically in the number of electrodes. It works for purely real or imaginary admittivity, (ERT or ECT), and for Magnetic Induction Tomography for real conductivity. It is not known if it can be applied to the complex case and it requires the voltage on current carrying electrodes.

Linear sampling methods [22, 124, 66] have a similar time complexity and advantages as the monotonicity method. While still applied to piecewise constant conductivities, linear sampling methods can handle any number of discrete conductivity values provided the anomalies separated from each other by the background. The method does not give an indication of the conductivity level but rather locates the jump discontinuities in conductivity. Both monotonicity and linear sampling methods are likely to find application in situations where a small anomaly is to be detected and located, for example breast tumours.

Finally a challenge remains to recover anisotropic conductivity which arises in applications from fibrous or stratified media (such as muscle), flow of non-spherical particles (such as red blood cells), or from compression (for example

in soil). The inverse conductivity problem at low frequency is known to suffer from insufficiency of data, but with sufficient *a priori* knowledge (for example [86]) the uniqueness of solution can be restored. One has to take care that the imposition of a finite element mesh does not predetermine which of the family of consistent solutions is found [112]. Numerical reconstructions of anisotropic conductivity in a geophysical context include [109], although there the problem of non-uniqueness of solution (diffeomorphism invariance) has been ignored. Another approach is to assume piece-wise constant conductivity with the discontinuities know, for example from an MRI image, and seek to recover the constant anisotropic conductivity in each region [51],[52].

1.13 Practical Applications

We have presented an overview of EIT reconstruction algorithms, but a question remains as which techniques will be usefully applied to clinical problems in EIT. The major algorithms presented here have all been tested on tank data. Yorkey [155] compared Tikhov regularizied Gauss-Newton with *ad hoc* algorithms on two dimensional tanks, Goble [58, 59] and Metherall [96, 95] applied one step regularized Gauss-Newton to 3D tanks. P Vauhkonen [144, 147] applied a fully iterative regularized Gauss-Newton method to 3D tank data using the complete electrode model. More recently the linear sampling method [124] and the scattering transform method [99] have been applied to tank data. However there is a paucity of application of non-linear reconstruction algorithms to *in vivo* human data.

Most of the clinical studies in EIT assume circular or other simplified geometry and regular placement of electrodes. Without the correct modelling of the boundary shape and electrode positions [85] the forward model can not be made to fit the data by adjusting an isotropic conductivity. A non-linear iterative reconstruction method would therefore not converge, for this reason most clinical studies have used a linearization of the forward problem and reconstruct a difference image from voltage differences. This linearization has been regularized in various ways both *ad hoc* methods such as those used by the Sheffield group [8, 9] and systematic such as the NOSER method [32] of RPI. Studies of EIT on the chest such as [100, 135, 74] assume a 2D circular geometry, although some attempts have been made to use a realistic chest shape [84]. Similar simplifications have been made for EIT studies of the head and breast. Three dimensional linear reconstruction algorithms have been applied to the human thorax [95] although three dimensional measurement has not become common place *in vivo* due to the difficulty of applying and accurately positioning large numbers of individual electrodes. One possible solution for imaging objects close to the surface is to employ a rigid rectangular array of electrodes. This is exactly the approach taken by the TransScan device [94] which is designed for the detection of nreast tumour, although reconstructions are essentially what geophysicists would call 'surface resistivity mapping', rather than tomographic reconstruction. Reconstruction of three dimensional EIT im-

ages from a rectangular array using NOSER-like method has been demonstrated *in vitro* by Mueller *et al* [97], and *in vivo* on the human chest using individual electrodes [98]. If the array is sufficiently small compared to the body, this problem become identical to the geophysical EIT problem [92] using surface (rather than bore-hole) electrodes.

The EIT problem is inherently non-linear. There are of course two aspects of linearity of a mapping. In engineering terminology: that the output scales linearly with the input, and that the principle of superposition applies. The lack of scaling invariance manifests itself in EIT as the phenomena of saturation, which means the linearity must be taken in to account to get accurate conductivity images. For small contrasts in conductivity, linear reconstruction algorithms will typically find a few isolated small objects, but underestimate their contrast. For more complex objects, even with small contrasts the lack of the superposition property means that linear algorithms cannot resolve some features. A simple test can be done in a tank experiment. With two test objects with conductivity σ_1 and σ_2 one can test if $\mathbf{Z}(\sigma_1) + \mathbf{Z}(\sigma_2) = \mathbf{Z}(\sigma_1 + \sigma_2)$ within the accuracy of the measurement system. If not then it is certainly worth using a non-linear reconstruction algorithm. However to use a non-linear algorithm the forward model used must be able to fit the data accurately when the correct conductivity is found. This means that the shape, electrode position and electrode model must all be correct. Until an accurate model is used, including a method of constructing accurate body shaped meshes and locating electrodes is perfected, it will not be possible to do justice to the EIT hardware by giving the reconstruction algorithms the best chance of succeeding. Fortunately work is proceeding in this direction [12, 54] and we are optimistic that non-linear methods will soon be commonplace for *in vivo* EIT.

Bibliography

[1] Astala K, and Paivarinta L, 2003, Calderón's inverse conductivity problem in the plane. Preprint.

[2] Alessandrini G, Isakov V. Powell J, 1995, Local uniqueness of the inverse conductivity problem with one measurement, Trans Amer Math Soc, 347, 3031-3041.

[3] Andersen KD and Christiansen E, 1995, A Newton barrier method forminimizing a sum of Euclidean norms subject to linear equality constraints. Technical Report, Department of Mathematics and Computer Science, Odense University, Denmark.

[4] Andersen KD, Christiansen E, Conn A, and Overton ML, 2000, An efficient primal-dual interior-point method for minimizing a sum of Euclidean norms. SIAM J. on Scientific Computing, 22:243-262, 2000.

[5] Arridge S, 1999, Optical tomography in medical imaging Inverse Problems, 15, R41-93

[6] Arridge SR and Schweiger M, 1998, A gradient-based optimisation scheme for optical tomography, Optics Express, 2, 213–226.

[7] Barber CB, Dobkin DP, Huhdanpaa H, The quickhull algorithm for convex hulls, ACM Trans Math Software, 22, 469–483, 1996

[8] Barber D and Brown B, 1986, Recent developments in applied potential tomography-apt, in Information Processing in Medical Imaging, ed S L Bacharach (Amsterdam: Nijhoff) 106–121

[9] Barber DC and Seagar AD, 1987, Fast reconstruction of resistance images, Clin. Phys. Physiol. Meas., 8 No 4A, 47-54

[10] Barrodale I and Roberts FDK, 1978, An efficient algorithm for discrete linear approximation with linear constraints. SIAM J. on Numerical Analysis, 15, 603-611.

[11] Brown BH and Seagar AD, 1987 The Sheffield data collection system Clin. Phys. Physiol. Meas. 8 Suppl A 91-97

[12] RH Bayford, A Gibson, A Tizzard, AT Tidswell and DS Holder, 2001. Solving the forward problem for the human head using IDEAS (Integrated Design Engineering Analysis Software) a finite element modelling tool. Physiological Measurements, 22, 55-63.

[13] Borsic A, 2002, Regularization Methods for Imaging from Electrical Measurements, PhD Thesis, Oxford Brookes University.

[14] Borsic A, McLeod CN and Lionheart WRB, 2001, Total variation regularisation in EIT reconstruction 2nd World Congr. on Industrial Process Tomography (Hannover), 579 -587

[15] Borsic A, Lionheart WRB, McLeod CN, 2002 Generation of anisotropic-smoothness regularization filters for EIT, IEEE Transactions of Medical Imaging, 21, 596 -603.

[16] Babuska I, and Strouboulis T, 2001, The Finite Element Method and its Reliability, (Oxford: Oxford University Press)

[17] Barrett R et al, 1994, Templates for the Solution of Linear Systems: Building Blocks for Iterative Methods, 2nd Edition, SIAM, Philadelphia, or online at `ftp://ftp.netlib.org/templates/templates.ps`

[18] Borcea L, 2001, A nonlinear multigrid for imaging electrical conductivity and permittivity at low frequency Inverse Problems 17 329-359

[19] Bertero M and Boccacci P, 1998, Introduction to Inverse Problems in Imaging. IOP Publishing Ltd., London.

[20] Aster R, Borchers B, Thurber C, 2004, Parameter Estimation and Inverse Problems, Academic Press.

[21] Bossavit A, 1998, Computational Electromagnetism, Variational formulations, Edge elements, Complementarity, (Boston: Academic Press).

[22] Brühl M, 2001, Explicit Characterization of Inclusions in Electrical Impedance Tomography, SIAM J. Math Anal, 32, 1327-1341

[23] Breckon, W R, Pidcock, M K, Some Mathematical Aspects of Impedance Imaging, Mathematics and Computer Science in Medical Imaging, Ed Viergever and Todd-Pokropek, NATO ASI series F, Vol 39, Springer, 351-362.

[24] Breckon WR, 1990, Image Reconstruction in Electrical Impedance Tomography, Ph.D. Thesis, Oxford Polytechnic.

[25] Breckon WR and Pidcock MK, 1988, Data errors and reconstruction algorithms in electrical impedance tomography Clin. Phys. Physiol. Meas. 9 No 4A, 105-109

[26] Breckon WR., Measurement and reconstruction in electrical impedance tomography, in 'Inverse problems and imaging', Ed. G.F. Roach, Pitman Res. Notes in Math., 245 , pp1-19, 1991.

[27] Byars M, 2001, Developments in Electrical Capacitance Tomography, Proc. World Congress on Industrial Process Tomography, Hannover, 542-549.

[28] Calderón AP, 1980, On an inverse boundary value problem. In Seminar on Numerical Analysis and Its Applications to Continuum Physics, pp. 67-73, Rio de Janeiro, Sociedade Brasileira de Matematica.

[29] D. Calvetti, L. Reichel and A. Shuibi, 2003, Enriched Krylov subspace methods for ill-posed problems, Linear Algebra Appl., 362 , 257-273

[30] Chan TF, Golub G, and Mulet P, 1995, A nonlinear primal dual methodfor TV-based image restoration. UCLA CAM Report 95-43.

[31] Chan TF, Tai X, 2004, Level set and total variation regularization for elliptic inverse problems with discontinuous coefficients, J Comp Physics, 193, 40–66.

[32] Cheney, M, Isaacson D, Newell JC, Simske S and Goble J, 1990, NOSER: An algorithm for solving the inverse conductivity problem. Int. J. Imaging Systems & Technology 2, 66-75.

[33] COMSOL, The FEMLAB reference manual, COMSOL AB, Stockholm, 2000.

[34] Cheng K, Isaacson D, Newell JC and Gisser DG, 1989 Electrode models for electric current computed tomography IEEE Trans. on Biomedical Engineering 36 918-24

[35] M. Cheney, and D. Isaacson, Distinguishability in Impedance Imaging, IEEE Trans. Biomed. Eng., 39, pp. 852-860, 1992.

[36] Chung ET, Chan TF and Tai XC, 2003, Electrical Impedance Tomography Using Level Set Representation and Total Variational Regularization, UCLA Computational and Applied Mathematics Report 03-64.

[37] Cook RD., Saulnier GJ, Gisser DG, Goble JC, Newell JC and Isaacson D., 1994, ACT 3: A high speed high precision electrical impedance tomograph. IEEE Trans. Biomed. Eng. 41, 713-722.

[38] Coleman TF and. Li Y, 1992, A globally and quadratically convergentaffine scaling method for linear problems. SIAM J. on Optimization,3, 609-629.

[39] Colin de Verdière Y, Gitler I, Vertigan, D, 1996, Réseaux électriques planaires II, Comment. Math. Helv., 71, 144–167.

[40] EB Curtis, JA Morrow, Inverse Problems for Electrical Networks, Series on Applied Mathematics - Vol. 13, World Scientific, Singapore, 2000

[41] Colton D, Kress R, 1998, Inverse Acoustic and Electromagnetic Scattering Theory, 2nd edition, Springer, Berlin.

[42] Ciulli S, Ispas S, Pidcock MK, Stroian A, 2000 On a mixed Neumann-Robin boundary value problem in electrical impedance tomography, Z Angewandte Math Mech 80, 681-696

[43] Dobson DC and Vogel CR, 1997, Convergence of an iterative method for total variation denoising. SIAM J. on Numerical Analysis, 43, 1779-1791.

[44] Dorn O , Miller El, Rappaport CM, 2000, A shape reconstruction method for electromagnetic tomography using adjoint fields and level sets, Inverse Problems 16, 1119-1156.

[45] Engl HW, Hanke M, Neubauer A, 1996, Regularization of Inverse Problems, Kluwer, Dordrecht 1996,

[46] Eyüboğlu BM and Pilkington TC, 1993, Comment on Distinguishability in Electrical-Impedance Imaging, IEEE Trans. Biomed. Eng., 40, 1328-1330

[47] Fletcher R, Reeves C,1964,, Function minimization by conjugate gradients, Computer J. 7 (1964) 149–154.

[48] Folland GB 1995, Introduction to Partial Differential Equations. Second Edition, Princeton Univ Press.

[49] Fox C and Nicholls G, 1997, Sampling conductivity images via MCMC, in "The Art and Science of Bayesian Image Analysis", K. Mardia, R. Ackroyd, and C. Gill, eds., Leeds Annual Statistics Research Workshop, pp. 91– 100, University of Leeds.

[50] George A, and Liu J, 1989, The Evolution of the Minimum Degree Ordering Algorithm, SIAM Review, 31, 1-19.

[51] Glidewell ME, Ng KT, 1997, Anatomically constrained electrical impedance tomography for three-dimensional anisotropic bodies, IEEE Trans. Med. Imaging, 16, 572-580.

[52] Gong L, Zhang KQ, Unbehauen R, 1997, 3-D anisotropic electrical impedance imaging, IEEE Trans Magnetics, 33, 2120-2122.

[53] Gilbert JR , Moler C, and Schreiber R, 1992, Sparse Matrices in MATLAB: Design and Implementation, SIAM Journal on Matrix Analysis and Applications 13, 1992, pp. 333-356.

[54] A P Gibson, J Riley, M Schweiger, J C Hebden, S R Arridge and D T Delpy, 2003, A method for generating patient-specific finite element meshes for head modelling, Phys. Med. Biol. 48 481-495

[55] Gisser DG, Isaacson D and Newell JC, Current topics in impedance imaging, Clin. Phys. Physiol. Meas., 8 Suppl A, pp39–46, 1987.

[56] Gisser DG , Isaacson D and Newell JC, 1990, Electric Current computed-tomography and eigenvalues, SIAM J. Appl. Math., 50 1623-1634.

[57] Giusti E, 1984. Minimal Surfaces and Functions of Bounded Variation.Birkhauser.

[58] Goble J and Isaacson D, 1990, Fast reconstruction algorithms for three-dimensional electrical impedance tomography, Proc. IEEE-EMBS Conf, 12(1) 100-101.

[59] Goble J, 1990, The three-dimensional inverse problem in electric current computed tomography, PhD thesis, Rensselaer Polytechnic Institute, NY, USA

[60] Dobson DC and Santosa F, 1994, An image enhancement technique for-electrical impedance tomography. Inverse Problems, 10, 317-334, 1994.

[61] Golub GH and Van Loan CF, 1996, Matrix Computations, 3rd ed. (Baltimore, MD: Johns Hopkins University Press).

[62] Greenleaf, A and Uhlmann G, 2001, Local uniqueness for the Dirichlet-to-Neumann map via the two-plane transform. Duke Math. J. 108, 599–617.

[63] Haber E, Ascher UM, 2001 Preconditioned all-at-once methods for large, sparse parameter estimation problems, Inverse Problems, 17, 1847-1864

[64] Hagger WW, 2000, Iterative methods for nearly singular linear systems, SIAM J Sci Comp,22, 747-766.

[65] Hanke M. 1995, Conjugate gradient type methods for ill-posed problems, Pitmannresearch notes in mathematics, Longman, Harlow Essex.

[66] Hanke M, Brühl M, 2003, Recent progress in electrical impedance tomography, Inverse Problems, 19, S65-S90

[67] Hansen PC, 1998, Rank-deficient and discrete ill-posed problems: numerical aspects of linear inversion, (Philadelphia: SIAM).

[68] Hettlich F and Rundell W, 1998 The determination of a discontinuity in a conductivity from a single boundary measurement Inverse Problems 14 67-82

[69] Heikkinen LM, Vilhunen T, West RM and Vauhkonen M, 2002, Simultaneous reconstruction of electrode contact impedances and internal electrical properties: II. Laboratory experiments Meas. Sci. Technol. 13, 1855-1861

[70] Higham NJ, 1996, Accuracy and stability of numerical algorithms, SIAM, Philadelphia.

[71] Hoerl AE, 1962, Application of ridge analysis to regression problems. Chemical Engineering Progress, 58, 54-59.

[72] Ingerman, D, Morrow, JA, 1998, On a characterization of the kernel of the Dirichlet-to-Neumann map for a planar region, SIAM J. Math. Anal, 29, 106–115

[73] Isaacson D, 1986, Distinguishability of conductivities by electric-current computed-tomography, IEEE Trans. Med. Imaging 5, 91-95.

[74] Isaacson, D, Newell JC, Goble JC and Cheney M, 1990,Thoracic impedance images during ventilation. Proc. IEEE-EMBS Conf. 12(1), 106-107.

[75] Isakov V, 1997, Inverse Problems for Partial Differential Equations, Springer, 1997

[76] Kaipio J, Kolehmainen V, Somersalo E and Vauhkonen M, 2000, Statistical inversion and Monte Carlo sampling methods in electrical impedance tomography, Inverse Problems 16 1487-1522.

[77] Ki H and Shen D, 2000, Numerical inversion of discontinuous conductivities, Inverse Problems, 16, 33–47.

[78] Kohn RV, Vogelius M, 1985, Determining conductivity by boundary measurements. II. Interior results. Comm. Pure Appl. Math. 38, 643–667.

[79] A. Köksal and B. M. Eyüboğlu, 1995, Determination of optimum injected current patterns in electrical impedance tomography, Pysiol Meas 16, ppA99-A109.

[80] Kolehmainen K, Arridge SR, Lionheart WRB, Vauhkonen M and Kaipio JP, 1999, Recovery of region boundaries of piecewise constant coefficients of elliptic PDE from boundary data, Inverse Problems 15, 1375-1391

[81] Kolehmainen V, Vauhkonen M, Kaipio JP and Arridge SR, 2000, Recovery of piecewise constant coefficients in optical diffusion tomography, Optics Express 7, 468-480.

[82] Kolehmainen V, 2002, Novel Approaches to Image Reconstruction in Diffusion Tomography. PhD thesis, Department of Applied Physics Kuopio University.

[83] Kotre C J 1989 A sensitivity coefficient method for the reconstruction of electrical impedance tomograms Clin. Phys. Physiol. Meas. 10 275-81

[84] Lionheart WRB *et al*, 1997 , Electrical Impedance Tomography for high speed chest imaging, Physica Medica, Vol 13, Suppl 1, 247-24.

[85] Lionheart WRB, 1999, Uniqueness, shape, and dimension in EIT, Annals New York Acad. Sci., 873, 466-471

[86] Lionheart WRB, 1997, Conformal uniqueness results in anisotropic electrical impedance imaging. Inverse Problems,13, 125-134.

[87] Lionheart WRB, Kaipio J, McLeod CN, 2001, Generalized optimal current patterns and electrical safety in EIT, Physiol. Meas., 22, 85-90

[88] Lionheart WRB, 2004, Developments in EIT reconstruction algorithms: pitfalls, challenges and recent developments, to appear in special issue Physiol Meas, 2004

[89] Loke MH and Barker R, 1996. Rapid least-squares inversion of apparent resistivity pseudosections by a quasi-Newton method: Geophysical Prospecting, 44, 131-152.

[90] Loke MH and Barker RD, 1996, Practical techniques for 3D resistivity surveys and data inversion, Geophysical Prospecting, 44, pp. 499-523.

[91] Lovell JR, 1993, Finite Element Methods in Resistivity Logging, PhD Thesis, Delft University of Technology.

[92] Lukaschewitsch M, Maass P and Pidcock M, 2003 Tikhonov regularization for electrical impedance tomography on unbounded domains, Inverse Problems 19, 585-610.

[93] Martin T and Idier J, 1998, Stability and accuracy of finite element direct solvers for electrical impedance tomography, Tech. rep., L2S.

[94] Malich A *et al*, 2000, Electrical impedance scanning for classifying suspicious breast lesions: first results European Radiology, 10, 1555-1561.

[95] Metherall P, Barber DC, Smallwood RH and Brown BH, 1996 , Three Dimensional Electrical Impedance Tomography, Nature 380, 509-512.

[96] Metherall P, 1998, Three Dimensional Electrical Impedance Tomography of the Human Thorax, PhD thesis, University of Sheffield.

[97] Mueller J, Isaacson D, Newell J, 1999, A Reconstruction Algorithm for Electrical Impedance Tomography Data Collected on Rectangular Electrode Arrays, J. Mueller, D. Isaacson, and J. Newell, IEEE Trans. Biomed. Engineering, 46, 1379-1386.

[98] Mueller JL, Isaacson D, Newell JC, 2001, Reconstruction of Conductivity Changes Due to Ventilation and Perfusion from EIT Data Collected on a Rectangular Electrode Array, Physiol. Meas., 22, 97-106

[99] Mueller J, Siltanen S, and Isaacson D, 2002, A Direct Reconstruction Algorithm for Electrical Impedance Tomography, IEEE Trans. Med. Imaging, 21, 555-559.

[100] McArdle FJ, Suggett AJ, Brown BH and Barber DC, 1988, An assessment of dynamic images by applied potential tomography for monitoring pulmonary perfusion, Clin. Phys. Physiol. Meas., 9 No 4A, 87-91

[101] McCormick S F and Wade J G, 1993 Multigrid solution of a linearized, regularized least-squares problem in electrical impedance tomography Inverse Problems 9 697 713

[102] Molinari M, Cox SJ, Blott BH, Daniell GJ, 2002, Comparison of algorithms for non-linear inverse 3D electrical tomography reconstruction, Physiol Meas 23, 95-104

[103] Molinari M, 2003, High Fidelity Imaging in Electrical Impedance Tomography, PhD Thesis, University of Southampton.

[104] Marquardt D. 1963, An algorithm for least squares estimation of nonlinear parameters. SIAM J. Appl. Math. 11, 431-441.

[105] Meng S, West R, Ackroyd R, 2004, Markov Chain Monte Carlo techniques and spatial-temporal, modelling for medical EIT, submitted to Physiol Meas.

[106] DF Morrison, Applied linear statistical methods, Prentice Hall, New Jersey, 1983

[107] Natterer F, 1982, The Mathematics of Comuterized Tomogrpahy, Wiley

[108] Nichols G, Fox C, 1998, Prior modelling and posterior sampling in impedance imaging, in "Bayesian Inference for Inverse Problems" ,ed. A. Mohammad-Djafari, Proc. SPIE 3459, 116–127

[109] Pain CC, Herwanger JV, Saunders JH, Worthington MH, de Oliveira CRE, 2003, Anisotropic resistivity inversion Inverse Problems, 19, 1081-1111

[110] Paulson K, Breckon W, Pidcock M Electrode Modeling In Electrical-Impedance Tomography SIAM J Appl Math, 1992, 52, pp.1012-1022

[111] Paulson KS, Lionheart WRB, Pidcock MK, POMPUS - An Optimized EIT Reconstruction Algorithm, Inverse Problems, 1995, 11,, pp.425-437.

[112] Perez-Juste Abascal JF, 2003,The Anisotropic Inverse Conductivity Problem, MSc Thesis, University of Manchester.

[113] Phillips DL, 1962, A technique for the numerical solution of certain integral equations of the first kind, J Assoc Comput Mach, 9, 84-97

[114] Player MA, van Weereld J, Allen AR, Collie DAL, 1999 Truncated-Newton algorithm for three-dimensional electrical impedance tomography, Electronics Letters, 35, 2189-2191

[115] Polydorides N and Lionheart WRB, 2002, A Matlab toolkit for three-dimensional electrical impedance tomography: a contribution to the Electrical Impedance and Diffuse Optical Reconstruction Software project, Meas. Sci. Technol. 13 1871-1883

[116] Polydorides N, 2002, Image Reconstruction Algorithms for Soft Field Tomography, PhD Thesis, UMIST.

[117] Polydorides N, Lionheart, WRB McCann, H, 2002, Krylov subspace itemacserative techniques: on the detection of brain activity with electrical impedance tomography. IEEE Trans Med Imaging, 21, 596 -603.

[118] Ramachandran P, 2004, The MayaVi Data Visualizer, **http://mayavi.sourceforge.net**

[119] Rondi L, Santosa F, Enhanced electrical impedance tomography via the Mumford-Shah functional, preprint.

[120] Rudin LI, Osher S, and Fatemi E, 1992, Nonlinear total variation basednoise removal algorithms. Physica D, 60, 259-268.

[121] Saad Y and Schultz MH, 1986, GMRES: A generalized minimal residual algorithm for solving nonsymmetric linear systems, SIAM J. Sci. Statist. Comput., 7, 856-869.

[122] Santosa F, 1995, A level-set approach for inverse problems involving obstacles, ESAIM Control Optim. Calc. Var. 1 (1995/96) 17-33

[123] Santosa F, Vogelius M, 1991, A backprojection algorithm for electrical impedance imaging, SIAM J. Appl. Math. 50, 216-243

[124] Schappel B, 2003, Electrical Impedance Tomography of the Half Space: Locating Obstacles by Electrostatic Measurements on the boundary, Proceedings of the 3rd World Congress on Industrial Process Tomography, Banff, Canada, September 2-5, 788-793.

[125] Schöberl J, 1997, NETGEN - An advancing front 2D/3D-mesh generator based on abstract rules, Comput. Visual .Sci, 1, 41-52,

[126] Seagar AD, 1983,, Probing with low frequency electric current, PhD Thesis, University of Canterbury, Christchurch, NZ, 1983.

[127] Siltanen S, Mueller J, Isaacson D, 2000, An implementation of the reconstruction algorithms of Nachman for the 2D inverse conductivity problem, Inverse Problems, 16, 681-699.

[128] Shimada K, Gossard DC, 1995, Bubble mesh: automated triangular meshing of non-manifold geometry by sphere packing, ACM Symposium on Solid Modeling and Applications archive Proceedings of the third ACM symposium on Solid modeling and applications table of contents Salt Lake City, Utah, USA, 409–419.

[129] Silvester PP and Ferrari RL, 1990, Finite Elements for Electrical Engineers, Cambridge University Press, Cambridge.

[130] Somersalo E, Cheney M, Isaacson D, Isaacson E, 1991, Layer Stripping, a Direct Numerical Method for Impedance Imaging, Inverse Problems, 7, 899–926

[131] Somersalo E, Isaacson D and Cheney M 1992 A linearized inverse boundary value problem for Maxwell s equations J. Comput. Appl. Math., 42, 123–136

[132] Somersalo E, Kaipio JP, Vauhkonen M, and D. Baroudi D. 1997 Impedance imaging and Markov chain Monte Carlo methods. Proc. SPIE's 42nd Annual Meeting, pages 175-185.

[133] Soleimani M, Powell C, 2004, Black-box Algebraic Multigrid for the 3D Forward Problem arising in Electrical Resistance Tomography, preprint.

[134] Somersalo E, Cheney M and Isaacson D, 1992,Existence and uniqueness for electrode models for electric current computed tomography. SIAM J. Appl. Math., 52, 1023-1040.

[135] Smallwood RD *et al*, 1999, A comparison of neonatal and adult lung impedances derived from EIT images Physiol. Meas., 20, 401-413

[136] Strang G, Introduction to Linear Algebra, 3rd Edition, 1988, Wellesley-Cambridge Press.

[137] Strang G, and Fix GJ, 1973, An Analysis of the Finite Element Method, Prentice-Hall, New York.

[138] Sylvester J and Uhlmann G 1986 A uniqueness theorem for an inverse boundary value problem n electrical prospection Commun. Pure Appl. Math. 3991-112

[139] Tamburrino A, Rubinacci G, 2002, A new non-iterative inversion method in electrical resistancetomography, Inverse Problems, 18, 2002

[140] A Tarantola, 1987, Inverse Problem Theory, Elsevier.

[141] A N Tikhonov Solution of incorrectly formulated problems andthe regularization method Soviet Math Dokl 4 1963, 1035-1038 English translation of Dokl Akad Nauk SSSR 151, 1963, 501-504

[142] Lassas M, Taylor M, Uhlmann G, 2003, The Dirichlet-to-Neumann map for complete Riemannian manifolds with boundary, Comm. Anal. Geom. 11, 207-222

[143] Vauhkonen, M.; Vadasz, D.; Karjalainen, P.A.; Somersalo, E.; Kaipio, J.P., 1998, Tikhonov regularization and prior information in electrical impedance tomographyIEEE Trans Medical Imaging, 19, 285-293

[144] Vauhkonen PJ, Vauhkonen M, Savolainen T, Kaipio JP, 1998, Static three dimensional electrical impedance tomography, Proceedings of ICEBI'98, Barcelona, Spain, 41 PaiviInfVauhkonen PJ, Vauhkonen M, Kaipio JP, 2000, Errors due to the truncation of the computational domain in static three-dimensional electrical impedance tomography. Physiol Meas, 21, 125-135.

[145] Vauhkonen M, Karjalainen PA, and Kaipio JP, 1998, A Kalman Filter approach to track fast impedance changes in electrical impedance tomography, IEEE Trans Biomed Eng, 45, 486-493.

[146] Vauhkonen M, 1997, Electrical Impedance Tomography and Prior Information, PhD Thesis, University of Kuopio.

[147] Vauhkonen PJ, 1999, Second order and Infinite Elements in Three-Dimensional Electrical Impedance Tomography, Phil.Lic. thesis, Department of Applied Physics, University of Kuopio, Finland, report series ISSN 0788-4672, report No. 2/99.

[148] Vauhkonen M, Lionheart WRB, Heikkinen LM, Vauhkonen PJ and Kaipio JP, 2001 A Matlab package for the EIDORS project to reconstruct two-dimensional EIT images Physiol. Meas. 22 107-11

[149] Mitchell S and Vavasis S, 2000, Quality Mesh Generation in Higher Dimensions, SIAM J. Comput. 29, 1334-1370.

[150] Mitchell SA and Vavasis SA. 2000, Quality mesh generation in higher dimensions. SIAM J. Comput., 29, 1334–1370.

[151] Vogel. C, 2001, Computational methods for inverse problems (Philadelphia: SIAM).

[152] Wade JG, Senior K and Seubert S, 1996 Convergence of Derivative Approximations in the Inverse Conductivity Problem, Bowling Green State University, Technical Report No. 96-14

[153] Yang WQ, Spink DM, York TA, McCann H, An image-reconstruction algorithm based on Landweber's iteration method for electrical-capacitance tomography, Meas. Sci. Tech. , 1999, 10, pp.1065-1069

[154] York T (ed), 1999, Proceedings of the 1st World Congress on Industrial Process Tomography, Buxton, UK, (Leeds: VCIPT)

[155] Yorkey TJ, Comparing Reconstruction Methods for Electrical Impedance Tomography 1986, PhD Thesis, Department of Electrical and Computational Engineering, University of Wisconsin, Madison, Wisconsin.

[156] Xue G and Ye Y, 2000,. An efficient algorithm for minimizing a sum ofpnorms. SIAM J. on Optimization, 10, 551-579.

[157] Zhu QS, McLeod CN, Denyer CW, Lidgey FJ and Lionheart WRB, 1994, Development of a real-time adaptive current tomograph Physiol. Meas. 15, A37-A43